**Response to Referee 1**

Review of "Characteristics of sub-10 nm particle emissions from in-use commercial aircraft observed at Narita International Airport" by Takegawa et al. This paper describes measurements of aircraft engine particle emissions during takeoff operations at Narita International Airport. Concentration measurements are made with two TSI condensation particle counters (CPC) with differing lower detection size limits (3 nm for the Model 3776 CPC and 7-10 nm for the Model 3771 CPC), and the difference between the particle concentrations measured by these counters is intepreted as the number concentration of sub-10-nm particles. In addition, a TSI Scanning Mobility Paricle Sizer (SMPS) and Engine Exhaust Particle Sizer (EEPS) are used to measure the size distribution of particles. A heated tube at 350 degrees Celsius is used to remove volatile particles so that the counters and SMPS can switch between measuring all particles or only the non-volatile particle fraction. The main finding of the paper is that there are significant differences between the particle concentrations measured by the 3776 counter versus the 3771 counter. Size distribution measurements for particle sizes greater than 10 nm are also presented to support the hypothesis that a significant fraction of the total and non-volatile particle number concentrations are below 10 nm; however, as the authors note, there are substantial particle diffusional losses at these sizes and the uncertainties and data corrections are significant!

Overall, the manuscript is well written and enjoyable to read. The underlying data are available in the supplementary information, which is excellent. The paper does a great job of characterizing the detection and penetration efficiences of the particle counters (although, I have a significant quibble with the use of the 3772 CPC to characterize the latter as discussed below). I previously reviewed a prior version of this manuscript for another journal, and I'm delighted to see that the authors have incorporated many of my comments/suggestions from that review into the present manuscript.

Observational reports of aircraft engine particle emissions in the literature are fairly limited given the large diversity in aircraft/engine types and airport conditions, and thus, this study is valuable in helping to overcome the current paucity of data. The content is appropriate for Atmospheric Chemistry and Physics. The paper may be publishable, but only if the following major comments are satisfactorily addressed:

We would like to thank the referee very much for giving us valuable comments and suggestions. We have revised the manuscript to address those comments and also made other corrections to improve the clarity of the presentation. The line numbers for this response letter are based on the manuscript with track changes.

1) On Lines 21-24, Lines 314-318, and elsewhere, the manuscript implies that it is somehow significant that the total particle number exceeds the number of non-volatile particles and that the regulatory emissions are somehow not accounting for these particles. This mischaracterizes the rationale behind the engine certification testing, which is designed to evaluate the emissions contributions from different engine types under relatively controlled conditions. It is well known that the volatile particle fraction is highly variable and depends on numerous variables including the fuel sulfur content and the environmental temperature. The regulatory focus on non-volatile particles attempts to remove some of this variability; although, there are still fuel composition impacts on soot formation that need to be accounted for. In sum, the comparison that the authors are making here is not an apples-to-apples comparison and is misleading. These sentences should be removed.

As the referee pointed out, the comparison with the regulatory standard was somewhat misleading. Our measurements indicate that the median values of the total and the non-volatile EI($N_{2.5}$) were $1.1 \times 10^{17}$ and $5.7 \times 10^{15}$ kg-fuel$^{-1}$, respectively, and the difference in these values (a factor of ~20) is interpreted as the average contribution of volatile particles. We have removed the description about the comparison with the engine exhaust measurements. We have also clarified in Section 1 that the SAE-ARP6320 has been developed for the certification of jet engine emissions and may not be directly compared with ambient measurement data.

Lines 26-31, 87-88, 433-439, 638-642

2) On Lines 25-26 it is stated that the mode diameters of the size distributions were found to be smaller than 10 nm in most cases, but this does not seem to be well established from Figure 9 (there are multiple curves where there is a discernable mode around 20 nm).

As the referee pointed out, there are multiple curves where there is a discernable mode around 20 nm. However, even for those curves, the maximum value is still found at ~10 nm in most cases (please see the plot in the next page). To quantitatively show this point, we compared the $d\mathrm{EI}(N)/d\log D$ values between each size bin for the individual take-off plumes shown in Fig. 8. We found that the $d\mathrm{EI}(N)/d\log D$ at the size bin of 10.8 nm exhibited the highest value for ~98% of the plumes. We also found that the $d\mathrm{EI}(N)/d\log D$ at 10.8 nm was more than two times larger than that at 14.3 nm for 79% of the plumes. These results suggest that the $d\mathrm{EI}(N)/d\log D$ values tended to increase with decreasing particle diameters around 10–20 nm and that the mode diameters of the $d\mathrm{EI}(N)/d\log D$ for the nucleation mode were smaller than 10 nm for the majority of the plumes observed in this study.

Lines 516-521

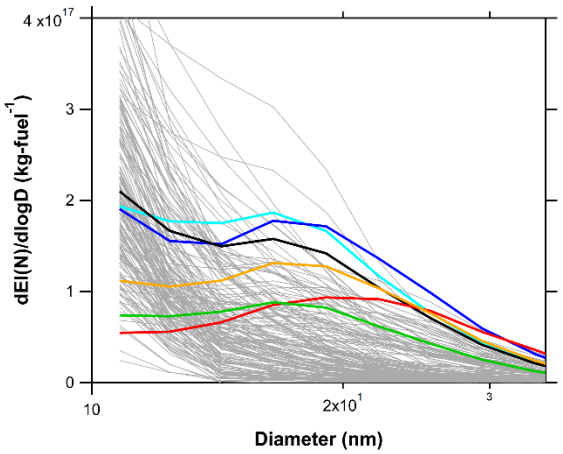


3) On Lines 27-29, it is suggested that the present paper "provides new insights into the significance of sub-10 nm particles..." that are important for human health and aviation emissions inventories. I'm not sure what these puported new insights are. The present study seems to be confirming extensive past literature that has found large emissions of volatile particles (thought to be organics and sulfuric acid), but these particles may or may not have a significant impact on health. This impact would depend on their solubility – if they are soluble, then the health impact would follow dose toxicity (which would be pretty insignificant). If they are insoluble, then they could penetrate the lungs and be important. Not all ultrafine particles are created equal here. Regarding the second point about emissions inventories – how important are these particles? They are likely to be rapidly depleted via coagulation processes, and so the number-based emissions of these sub-10 nm particles are likely to be very different even at the end of the runway as compared to the surrounding area. The strength of this statement regarding the impact of the present study needs to be toned down considerably.

To our understanding, the impacts of sub-10 nm particles from aviation on climate and human health are still uncertain. Righi et al. (2013, 2016) performed global model simulations and showed that the climate impacts of aviation on aerosols were sensitive to the parameterization of nucleation-mode particles (<~20 nm) in their model. In our view, the contribution of aircraft emissions to the number concentration of nucleation or Aitken mode particles is poorly understood. Sub-10 nm particles could be efficiently deposited in the olfactory mucosa, and the subsequent translocation of solid particles along the axons of the olfactory nerve might be a concern (Oberdörster et al., 2005). The health impacts of UFPs emitted from aircraft have not been well established, as pointed out by Ohlwein et al. (2019). We have added these points in Section 1.

Line 49-68

The primary importance of aviation-produced aerosol particles in assessing the climate impacts may be limited to the upper troposphere, and our results may not be directly transferred to the particle emissions at cruising altitudes. Nevertheless, field measurements near airports would contribute to

better understanding of aircraft emissions at cruising altitudes if they are properly integrated with engine tests and/or in-flight observations. To clarify this point, we also added the importance of integrating multiple platforms for better understanding of aircraft emissions in Section 1.

Line 102-109

4) I don't think there is support for the statement made on Line 34 that aircraft emissions somehow don't participate in any wet removal processes.

We have removed the sentence (Line 47-48).

5) I agree with the authors' statement on Line 70 that the technical issues associated with particle transport and losses of sub-10 nm particles need to be properly considered. How are these technical issues addressed in the present study? On Line 128-129, it is mentioned that the diffusional loss corrections within AIM are used, but these only apply to the SMPS system itself (not the 3m sampling lines or other flow splits and particle treatments). What corrections were applied to the concentration and size distribution data? Do these corrections drive the conclusions of the present paper, or are the findings the same even if the corrections are neglected?

The overall penetration efficiencies of particles through the sampling tubes were estimated by using the theoretical formulae proposed by Gormley and Kennedy (1949). We have added the details of the calculation procedures in Section S1 of the Supplement. Furthermore, we have added descriptions about the diffusion correction by the AIM software in Section S2 of the Supplement.

Sections S1-S2 of the Supplement

The corrections for the penetration efficiencies through the sampling tubes and the detection efficiencies were not incorporated in the UCPC and CPC data presented in Sections 3.2.1–3.2.4 because the actual size distributions in the sub-10 nm size range were uncertain. Furthermore, the corrections for the penetration efficiencies were not incorporated in the SMPS and EEPS data presented in Sections 3.2.2–3.2.3 for consistency with the UCPC/CPC data. We considered the effects of particle diffusion loss as systematic uncertainties (the error bars in Figs.6 and 7). The overall size dependency (i.e., increasing particle number concentrations with decreasing diameters below 20 nm) is consistent between the SMPS and EEPS data, regardless of the corrections.

On the other hand, we considered the penetration efficiencies and the detection efficiencies for estimating the size distributions of particle number EIs in Sections 3.2.5 and 4. This allows quantitative comparison with the particle number EIs reported by previous studies.

Lines 197-213

6) Is it reasonable to assume that the particle residuals leaving the thermal denuder are 1 nm? What about if they were 3 nm? or 5 nm? How robust are the paper's findings to this major assumption?

We estimated potential artifacts due to the nucleation of gaseous compounds vaporized from particles in the evaporation tube (nucleation artifacts). We assumed an initial cluster size of 1 nm, which approximately corresponds to the critical cluster size of sulfuric acid. As the referee pointed out, other potential artifacts may originate from the condensational growth of non-volatile particles (or residual particles downstream of the evaporation tube) smaller than the detectable size range of the UCPC (diameter < 2 nm). For example, residual particles with diameters of ~2 nm may grow to ~3 nm at an ambient mass concentration of 50 μg $m^{-3}$. However, this effect is significant only in the presence of a large fraction of non-volatile particles with diameters below 2 nm.

Lines 215-216, 249-252

7) I think it's great that the detailed removal efficiency tests described on Lines 221-222 were completed, but I question the use of the 3772 CPC as the detector since it doesn't rule out the possiblity that the particles didn't completely evaporate and would still be detectable by the 3776 CPC. If possible, it would be important to redo these experiments with the 3776 since the difference between the two CPCs is being used to infer the presence of sub-10-nm non-volatile particles.

We performed additional laboratory experiments by using the UCPC. The remaining fractions for 30 nm particles were found to be ~0.3% and <0.1% for the UCPC and CPC, respectively. The remaining fractions for 50 nm particles were found to be ~5% and <0.1% for the UCPC and CPC, respectively. These results suggested that about 5% of the 50 nm $C_{40}H_{82}$ particles might not have fully vaporized but shrunk to sizes between 2.5 and 10 nm downstream of the evaporation tube.

However, under the field measurement conditions, residues of >50-nm particles were likely negligible compared with the observed sub-10 nm non-volatile particles because the particle number concentrations for a diameter range of >50 nm measured by the EEPS (unheated) were far below the observed values of the 350°C heated $N_{2.5} - N_{10}$ (Fig. 7a). In addition, residues of 30–50 nm particles in the sub-10 nm size range after the evaporation tube were likely minor compared with the observed sub-10 nm non-volatile particles considering the sharp decrease in the $dN/d\log D$ values from 30 to 50 nm as measured by the EEPS (the remaining fractions were ~0.3% and 2% for 30 and 43 nm $C_{40}H_{82}$ particles, respectively).

We appreciate the referee very much for encouraging us to perform additional laboratory experiments. We consider that the discussion has become clearer compared to the previous version.

Lines 278-285, 307-320

8) I don't understand what is being referred to by the statement on Line 293 about the abscence of an "artificial nucleation mode". Please clarify.

We meant that the size dependency of non-volatile particles (gradual increasing trends with decreasing particle diameters from 100 to 15 nm) is unlikely to be explained by the artificial growth of particles downstream of the evaporation tube because the mass concentrations of aerosols in the plumes would not have been sufficient to yield particle growth exceeding 1 nm.

Lines 406-411

9) On Line 381 replace "soot" with "non-volatile"

Corrected (Line 587).

10) On Line 386, strike the "s" from the word "evidences"

Corrected (Line 585).

11) The sentence on Lines 391-393 speculating about rapid dilution prempting the growth of soot particles is unfounded and should be removed.

We have removed the sentence (Lines 597-599).

12) The discussion on take-off particle number concentration impacts on aircraft cruising altitudes on Line 423 does not seem relevant to the present paper.

This is related to the comment 3). As the referee pointed out, the results of this study may not be directly transferred to the particle emissions at cruising altitudes. We have moved this paragraph to the end of Section 4.2 (discussion) as an implication. Nevertheless, field measurements near airports would contribute to better understanding of aircraft emissions at cruising altitudes if they are properly integrated with engine tests and/or in-flight observations.

Lines 622-630

To clarify this point, we also added the importance of integrating multiple platforms for better understanding of aircraft emissions in Section 1. Field measurements of advected (diluted) aircraft exhaust plumes near runways are not optimal for obtaining systematic emission data, whereas potential artifacts associated with long sampling lines and/or high concentrations of condensable materials can be reduced by this approach. Furthermore, a variety of exhaust plumes from different types of in-use aircraft engines can be collectively characterized by field measurements near runways. Considering that the accessibility to platforms for sampling fresh engine exhausts (engine test cells, aircraft hangers, and runways) is generally restricted, these approaches should be complementarily selected for better characterizing UFP emissions from aircraft. Consistent integration of the data is also important for constructing reliable emission inventories from the

aviation sectors for the global troposphere (cruising altitudes), where the accessibility to sampling platforms is extremely limited.

Lines 102-109

13) Please change the y-axis scaling for the lower-left panels of Figures 7-8 to a linear scale to clearly show the agreement between the measurements of the smaller number mode. The contribution of the larger modes are already well captured by the dV/dlogDp

We have changed the y-axis for the total particle $dN/d\log D$ to a linear scale, as the referee suggested. We would like to keep the log scale for the non-volatile particle $dN/d\log D$ because the absolute values differed by an order of magnitude between the EEPS and SMPS.

Figures 6 and 7 in the revised version

14) From the inset of Figure 9a it looks like there's the beginning of a hump in the gray curves that is reflected by the black line, but in Figure 10c this doesn't seem to be the case. What is the arbitrary units scale in Figure 10c and how were these different quantitative data scaled together?

We have changed the sensitivity calculations to obtain quantitative estimates of the $d\mathrm{EI}(N)/d\log D$. The GMD and GSD values assumed in Eq. (4) were used for the $d\mathrm{EI}(N)/d\log D$ in Eq. (5). The calculated $\mathrm{EI}(N_{2.5})$ was compared with the median $\mathrm{EI}(N_{2.5})$ derived from the observations to retrieve the absolute values of $d\mathrm{EI}(N)/d\log D$ and $\mathrm{EI}(N)$. The retrieved $d\mathrm{EI}(N)/d\log D$ values were found to be consistent with those derived from the EEPS (Fig. 8), which supports the validity of our estimate.

We appreciate the referee very much for this comment. We consider that the discussion has become clearer as compared to that in the previous version.

Line 540-576, Figures 9 and 10

**Response to Referee 2**

This paper reports the characteristics of sub-10nm particle emissions from field measurements at the Narita International Airport in Tokyo, Japan. Total and non-volatile particle emissions were measured using particle counting and size distribution instruments.

The paper is well written, and includes relevant details and analysis. I found some of the observations and results presented were not put into proper context with previous findings from earlier studies reported in the literature. Recent studies were cited, but their relevance to the current work was not well stated or in some cases was overstated. There are also some inconsistencies in the description of the results which requires clarification. I have several comments that I hope will help the authors in addressing the gaps identified.

We would like to thank the referee very much for giving us valuable comments and suggestions. We have revised the manuscript to address those comments and also made other corrections to improve the clarity of the presentation. The line numbers for this response letter are based on the manuscript with track changes.

General comments:

The introduction section needs to better state the motivation for this study. The authors provide good background and context for the study, but the motivation for investigating sub-10nm particles is lacking.

To our understanding, the impacts of sub-10 nm particles from aviation on climate and human health are still uncertain. Righi et al. (2013, 2016) performed global model simulations and showed that the climate impacts of aviation on aerosols were sensitive to the parameterization of nucleation-mode particles (<~20 nm) in their model. In our view, the contribution of aircraft emissions to the number concentration of nucleation or Aitken mode particles is poorly understood. Sub-10 nm particles could be efficiently deposited in the olfactory mucosa, and the subsequent translocation of solid particles along the axons of the olfactory nerve might be a concern (Oberdörster et al., 2005). The health impacts of UFPs emitted from aircraft have not been well established, as pointed out by Ohlwein et al. (2019). We have added these points in Section 1. Line 49-68

The primary importance of aviation-produced aerosol particles in assessing the climate impacts may be limited to the upper troposphere, and our results may not be directly transferred to the particle emissions at cruising altitudes. Nevertheless, field measurements near airports would contribute to better understanding of aircraft emissions at cruising altitudes if they are properly integrated with engine tests and/or in-flight observations. To clarify this point, we also added the importance of integrating multiple platforms for better understanding of aircraft emissions in Section 1.

Line 102-109

The difference between the total PM and non-volatile PM is the attributable to volatile PM. The formation of volatile PM is due to a number factors including ambient conditions, fuel used, etc. The authors while presenting data for total PM and non-volatile PM haven't made any observations about the volatile PM, which is some cases dominates.

As the referee pointed out, the particle number EIs were dominated by volatile particles. This point has been clarified in Sections 3.2.4 and 5. Based on offline chemical analysis, we have previously shown that jet engine lubrication oil was the major source of aerosol particles with diameters ranging from ~10 to 30 nm in air parcels observed during the measurement period (Fushimi et al., 2019). However, detailed analysis on the formation mechanisms of volatile particles was not performed in this study. This would be an important topic in future studies

Lines 437-439, 640-642

The study reports that the sub-10nm particles are non-volatile. Why is this different from earlier studies of aircraft engine emissions at airports? Is it because lower cut-off instruments were used or the mix of aircraft compared with previous studies is different, i.e. more newer engines in the fleet with different emissions characteristics or the fuel composition was different? The authors have not discussed the key finding from the current study in the context of previous observations.

The presentation of the results was ambiguous in the previous version. The major points of this manuscript are as follows:

- The median values of the total and the non-volatile EI($N_{2.5}$), which likely cover the major size range of aircraft emissions, were found to be $1.1 \times 10^{17}$ and $5.7 \times 10^{15}$ kg-fuel$^{-1}$, respectively. The difference in these values (a factor of ~20) is interpreted as the average contribution of volatile particles.
- More than half the total and the non-volatile particle number EIs in the aircraft take-off plumes were found in the size range smaller than 10 nm.

Therefore, the sub-10 nm particles were mostly volatile. The significance of sub-10 nm size ranges for the total particles was qualitatively consistent with previous studies, but that for the non-volatile particles was unexpected.

Lines 638-651

The key point in our results is that the non-volatile particle number and volume EIs originating from soot-mode particles (>20 nm) were much smaller than those reported by the previous studies for take-off plumes under real-world operating conditions (Lobo et al., 2012, 2015b; Moore et al., 2017a). This feature might be related to the significance of sub-10 nm non-volatile particles. The data presented by Moore et al. (2017a), which were obtained in 2014, exhibited lower contributions of soot-mode particles compared to those by Lobo et al. (2012, 2015b), which were obtained in

2005 and 2004, respectively. A possible explanation for this tendency is that newer engines might emit smaller non-volatile particles as compared with older engines, as the referee suggested.

Lines 607-613

The cut-off size of instruments is an important factor for the interpretation of the data, as the referee pointed out. However, detailed discussion on this point was not made because the information on the size dependent detection efficiencies for the instruments used in the previous studies were not available.

References: Include the weblink or doi for each for the references included in this paper.

We have added the doi numbers.

Specific comments:

(1) Lns 32-34: It is not clear how aircraft emissions are unique in this aspect compared to other transportation or emission sources. Are the authors referring to aircraft emissions during cruise? Rephrase this sentence.

We have removed the sentence (Lines 47-48).

(2) Lns 38-44: I think it is important to state that direct health impacts of UFP emitted from aircraft have not been currently established.

We have added this point (Lines 67-68). Please also see the answer regarding the significance of sub-10 nm particles (General comments).

(3) Lns 49-51: Ambient conditions also play an important role in the formation of volatile particles. Update the text accordingly.

Corrected (Line 76).

(4) Lns 72-73: A specific date for the measurements is stated in the introduction, however the next section (Ln 80) lists a range. Please be consistent.

Corrected (Lines 110-111).

(5) Lns 86-88: The authors state that the instruments used during the measurement at NRT have previously been used for airborne measurements. More pertinent to the discussion is how the instruments used in this study varied from earlier studies of aircraft emissions at airports.

The UCPC and CPC used for the field measurements were exactly the same as those used for airborne measurements in our previous studies, except for the dilution/heater sections.

Lines 125-127

(6) Ln 91: Specify the make and model of the NOx detector.

Corrected (Lines 130-131).

(7) Ln 131-132: The location of the EEPS was not indicated in Figure 2. Was the sample provided to the EEPS from the same inlet as that for the CPCs and SMPS? This should be stated in the manuscript.

The EEPS was operated independently from the UCPC/CPC/SMPS inlet system and it measured the unheated particle number size distributions during the entire period. The schematic of the inlet was added in Figure 2b.

Lines 178-183, Figure 2

(8) Lns 141-142: If the scanning time of the SMPS was set to 3 minutes, it is likely that the measured size distribution would be a combination of multiple plumes and not a single event. Other studies (Herndon et al., 2008; Lobo et al., 2012; Moore et al., 2017) have shown that plumes from an individual aircraft activity/movement are on the order of less than 1 minute.

The scanning time of the SMPS is an important issue. As described in Section 3.2.2, the time periods were carefully selected for investigating the effects of rapid changes in the particle number concentration during each SMPS scan on the derived particle size distribution. The SMPS needed ~30 s to scan the major population of particle number concentrations in the aircraft plumes (<30 nm). The EEPS data were averaged over 40 s around the timing of the SMPS scan corresponding to the diameter range of 15–30 nm (i.e., from 10 s before to 30 s after the onset of each SMPS scan).

Lines 361-366

(9) Lns 187-189: What size ranges did the different sources cover?

We have added the information on the particle size (EAG: 6–15 nm, CAST: 15–100 nm; and tube furnace particle generator: 15–30 nm). Lines 262-265

(10) Ln 190: "non-volatile propane soot particles supplied from the CAST" – What were the set points? Previous studies have shown a high volatile/organic content for certain the miniCAST set points, especially with pre-mixed nitrogen (e.g. Maricq, 2014; Durdina et al., 2016).

The CAST at AIST does not provide detailed information on the mixing ratios of gases (we just set the particle diameter). As the referee pointed out, internal mixtures of organic matters might be a concern. We put a tube furnace downstream of the CAST to remove organic compounds internally or externally mixed with soot. We used a volatility tandem DMA with a heater temperature of 350°C to confirm that the thermal treatment efficiently removed organic compounds; i.e., there was no significant difference in the mobility diameter of soot particles between the two DMAs.

Lines 265-268

(11) Lns 194-195: Instead of using qualitative phrases like “somewhat longer”, be specific in terms of the parameters.

The length of the sampling line for the CPC was ~90 cm. We have added this information.

Line 271

(12) Lns 218-220: It’s not clear why the penetration efficiency curve at room temperature was scaled. This should be explained and it should be noted in Figure 4 b) that these data are scaled.

The theoretical formulae proposed by Gormley and Kennedy (1949) requires the temperature profile in the sample air. Because the actual temperature profile of the sample air was uncertain at 350°C, it turned out to be difficult to perform a simple theoretical prediction of the penetration efficiency at 350°C. The description in the previous version was somewhat confusing. The penetration efficiency curve at 350°C (not shown in Fig. 3) was determined by scaling the calculated curve at 20°C with the experimental values at 350°C and at room temperature (~19–21°C) for larger diameters (>30, 50, and 100 nm).

Lines 301-306, Caption of Fig. 3

(13) Lns 233-234: This is not a fair comparison. The enhancement level for CO2 for individual plumes is not an indicator of similarity. For example, how would you compare if an air parcel has higher emissions closer to the engine but heavily diluted with ambient air vs. lower emissions closer to the engine but the plume is not as diluted? Both these cases could give the same CO2 enhancement, however, the residence time in the plume, and hence the opportunity for particles to nucleate, would be different in these two cases. Do you have any data to present this in the context of residence time in the plume?

The wind directions were east or east-southeast for Fig. 4a (average wind speed: 3.9 ± 0.7 m $s^{-1}$) and east or east-northeast for Fig. 4b (average wind speed: 4.3 ± 0.6 m $s^{-1}$), indicating that relatively stable winds from the direction of the runway were dominant. The ambient temperature was ~10°C for Fig. 4a and ~8°C for Fig. 4b. Although the characteristics of the plumes shown in Figs. 4a and 4b cannot be directly compared, the similarity in the wind conditions suggests that the ages of the plumes were comparable (~50 s for the plumes in Fig. 4a and ~45 s for those in Fig. 4b).

Lines 326-339

(14) Lns 245-252: What is the main message of this plot? Is it supposed to indicate what fraction of particles heated to 350C are below 10nm? A bar chart would be more relevant to illustrate this point.

We have added the median values of the $N_{10}/N_{2.5}$ ratios for each concentration bin (Fig. 5b). The scatterplot would be still useful to show the variability in the ratios. Therefore, we would like to keep the scatterplot in addition to the median plot. Lines 352-353, Fig. 5

(15) Lns 256-257: What was the lower size cut-off for the EEPS? Was it also 10nm? Is the data in Fig 7a from the SMPS or the CPC? The text indicates CPC but the figure heading has SMPS (unheated).

Although the particle diameter range detectable by the EEPS extended from ~6 to 520 nm, our laboratory experiments showed that the EEPS may significantly underestimate particle number concentrations below 10 nm. Reduced detection efficiencies of sub-10 nm particles can also be inferred from the EEPS data obtained by other researchers (Moore et al., 2017a). In this study we used the EEPS data for particle diameters larger than 10 nm. Therefore, the EEPS and CPC data may be directly compared. We have modified the figure heading accordingly.

Lines 183-188, Fig. 6

(16) Lns 270-275: This enhancement has been previously reported for measurements of exhaust plumes in the near field (Lobo et al., 2012; Timko et al., 2013; Beyersdorf et al., 2014; Trueblood et al., 2018). Based on the number and volume distributions, can any inferences be made with respect to the type of plume being sampled, i.e. idle, take-off?

In the enhancement event shown here, the particle volume size distributions appeared to be bimodal, but the larger mode was significantly affected by accumulation-mode particles in the background air. As described in the Supplement, the distance from the observation point to the taxiway was ~380 m and that to the gate was >800 m. We expected that aircraft emissions during idling would contribute to relatively broad, diffuse increases in aerosols and $CO_2$, which would be difficult to characterize. We also expect that aircraft emissions during take-off and landing would appear as spiked increases in aerosols and $CO_2$ at the observation point. Therefore, we assume that the observed enhancements of aerosols were mostly from take-off or landing. To avoid this ambiguity, we have extracted discrete take-off plumes and subtracted the background contributions (Fig. 8).

The references that the referee provided are helpful (Lobo et al., 2012; Timko et al., 2013; Beyersdorf et al., 2014; Trueblood et al., 2018). We have carefully checked these papers, and selected Lobo et al. (2012) as a suitable reference in this context. The sampling setup (deployed instruments and sampling location relative to the runways) and the analysis procedures (discrete plume analysis) of this study are similar to those of Lobo et al. (2012, 2015b) and Moore et al. (2017a). For the similarities and differences between those studies and our results, please see the answer to the comment (20).

(17) Ln 293: What does “artificial nucleation mode” mean?

We meant that the size dependency of non-volatile particles (gradual increasing trends with decreasing particle diameters from 100 to 15 nm) is unlikely to be explained by the artificial growth of particles downstream of the evaporation tube because the mass concentrations of aerosols in the

plumes would not have been sufficient to yield particle growth exceeding 1 nm.

Lines 406-411

(18) Lns 314-316: The SAE standard system for aircraft engine emissions measurements consists of several sections (diluter, 25m sampling line, etc) that were not included in this study. I don't think it's fair to say that the difference is between real-world conditions and regulatory measurements. The difference is between measured total particle number and non-volatile particle number, which gives a measure of the volatile particle number emissions.

As the referee pointed out, the comparison with the regulatory standard was somewhat misleading. Our measurements indicate that the median values of the total and the non-volatile EI($N_{2.5}$) were $1.1 \times 10^{17}$ and $5.7 \times 10^{15}$ kg-fuel$^{-1}$, respectively, and the difference in these values (a factor of ~20) is interpreted as the average contribution of volatile particles. We have removed the description about the comparison with the engine exhaust measurements. We have also clarified in Section 1 that the SAE-ARP6320 has been developed for the certification of jet engine emissions and may not be directly compared with ambient measurement data.

Lines 26-31, 87-88, 433-439, 638-642

(19) Lns 316-318: It's not clear what is meant by "standard engine tests". The SAE standard system is used for the emissions certification testing of aircraft engine emissions. The engines used in these tests do not have the wear and tear associated with in-use commercial aircraft engines. Also, the data on the nvPM emissions from the certification tests is not publicly available.

We initially considered that our non-volatile particle measurements can be compared with the engine exhaust measurements by the SAE protocol. However, as mentioned in the previous answer, it is not appropriate to refer the engine certification tests here. We have removed this sentence.

Lines 433-437

(20) Lns 324-337: Can any inferences be drawn between the previous studies and the current one, other than the emissions being in the same range? The ambient conditions, background PM, fuel, airport operations, etc during all of these studies are different. However, the particle number emissions all fall into a similar range.

As described in the answer to the comment (16), the sampling setup (deployed instruments and sampling location relative to the runways) and the analysis procedures (discrete plume analysis) of this study are similar to those of Lobo et al. (2012, 2015b) and Moore et al. (2017a). Therefore, it is worthwhile discussing the similarities and differences between those studies and our results.

The fuel sulfur content is an important parameter for the comparison with other studies. We do not have information on the sulfur content of the fuel that was actually used at NRT. Instead, we

analyzed fuel samples (Jet A-1) provided by a jet fuel company in Tokyo (Ishinokoyu, Co. Ltd.) (Saitoh et al., 2019b). The sulfur content of the fuel samples ranged from 30.4 to 440 parts per million by weight (ppmw). We assume that these values are representative of the sulfur content of jet fuels commercially available in Tokyo during the observation period.

Lobo et al. (2012) reported particle number and mass EIs measured 100–350 m downwind of the runways at Oakland International Airport in August 2005. The total particle number EIs for various types of engines under take-off conditions ranged from $4 \times 10^{15}$ to $2 \times 10^{17}$ kg-fuel$^{-1}$, which inclusively covered the 25–75 percentile range of the total EI($N_{2.5}$) from our measurements. The fuel sulfur content was estimated to be 240–395 ppmw.

Lobo et al. (2015b) reported the particle number and mass EIs measured near the jet engine exits and 100–350 m downwind of the runways at Hartsfield-Jackson Atlanta International Airport in September 2004. The total particle number EIs for various types of engines under take-off conditions ranged from $7 \times 10^{15}$ to $9 \times 10^{17}$ kg-fuel$^{-1}$, which again inclusively covered the 25-75 percentile range of total EI($N_{2.5}$) from our measurements. The information on the fuel sulfur content was not provided.

Moore et al. (2017a) reported the particle number and volume EIs for take-off plumes based on field observations conducted at Los Angeles International Airport (LAX) in May 2014. We calculated the median values (and the 25–75 percentile range) of the total and the non-volatile particle number EIs provided by Moore et al. (2017a) to be 4.6 (3.1–5.8) $\times 10^{16}$ and 2.1 (1.1–3.6) $\times 10^{15}$ kg-fuel$^{-1}$, respectively. The median and 25–75 percentile range of the total and the non-volatile EI($N_{10}$) from our measurements showed good agreement with those from Moore et al. (2017a). The sulfur content of the jet fuel samples collected at LAX ranged from 620 to 1,780 ppmw (average: 1,180 ppm).

Timko (2010) showed that the total particle number EIs in moderately diluted plumes exhibited a relatively weak dependence on the fuel sulfur content (<1,500 ppmw) under high thrust conditions for various types of engines. Provided that the fuel sulfur content was likely below ~1,500 ppmw for the previous studies (Lobo et al., 2012, 2015b; Moore et al., 2017a) and this study, it might not be the major factor affecting the variability in the emissions of volatile particles among these studies.

We consider that the referee's question is very important. The total and non-volatile particle number EIs derived from the UCPC and CPC fell in the same range as those from the previous studies for take-off plumes under real-world operating conditions (Lobo et al., 2012, 2015b; Moore et al., 2017a). However, the characteristics of the size distributions appeared to be significantly different. Specifically, the non-volatile particle number and volume EIs originating from soot-mode particles

(>20 nm) were much smaller than those reported by the previous studies. This feature might be related to the significance of sub-10 nm non-volatile particles. The data presented by Moore et al. (2017a), which were obtained in 2014, exhibited lower contributions of soot-mode particles compared to those by Lobo et al. (2012, 2015b), which were obtained in 2005 and 2004, respectively. A possible explanation for this tendency is that newer engines might emit smaller non-volatile particles as compared with older engines.

We have added the above points in Sections 3.2.4 and 4.2. We appreciate the referee very much for this comment. We consider that the discussion has become clearer.

Lines 459-492, 580-613

(21) Lns 337-342: Zhang et al., 2019 did not perform any measurements themselves but used the data from previous studies in their analysis. This reference should not be included in the comparison of measurement data. Also, Zhang et al. 2019 excluded certain datasets in their analysis, and thus limits the conclusions that can be drawn from their analysis. As stated previously, there are other measurements reported from previous studies that can be used to compare and quantify the differences or similarities with the current study.

We have removed Zhang et al. (2019) from the comparison (Lines 492-496).

(22) Lns 353-354: The three studies referenced here all reported bi-modal distributions. When referring to the mode diameter of particle number EIs measured downstream of the engine in the near field, a distinction between the nucleation and accumulation modes should be made. For the case here, the nucleation mode should be specified.

We have specified the nucleation mode when we discuss the mode diameter (Lines 514-523).

(23) Lns 354-360: This discussion does not follow from the previous comparisons. The authors state that the work by Kinsey et al., 2019 is an exception, but don't state how it impacted the mode diameter of particles. Aircraft engine emissions are known to vary with fuel composition and ambient conditions, but the authors do not state the relevance of these factors to their study.

As the referee pointed out, the discussion does not follow from the previous comparisons. The results from Kinsey et al. (2019) might not be directly compared with our results. We have removed the comparison.

Lines 531-537

(24) Lns 362-364: The size distributions presented thus far have been shown to be bimodal. Why was an assumption of log-normality made? Is the constraint only for the nucleation mode? Please be specific.

We assumed monomodal size distributions for $dN/d\log D$ and $dEI(N)/d\log D$ considering the shapes of the observed size distributions for total and non-volatile particles (Figs. 6 and 7). It is difficult to retrieve bimodal size distributions from the observations because the particle number concentrations were dominated by the smaller mode (we would not use "nucleation mode" for non-volatile particles because it might lead to confusion).

Lines 552-554

(25) Lns 386-393: While this section discusses the possible mechanisms for the production of sub-10nm particles in jet engine exhaust, it does not explain the difference observed in sub-10nm soot particles reported in earlier studies. The authors should expand upon this. Are the sub-10nm particles non-volatile metals or soot or both?

We have removed the discussion on the soot formation mechanisms because it was too speculative. Currently we do not have a direct evidence that the observed sub-10 nm non-volatile particles are composed mainly of soot. Our estimate implies the presence of very small non-volatile particles with diameters down to a few nanometers. This is not consistent with the size of the primary soot particles from jet engines estimated by using transmission electron microscopy (TEM) or laser-induced incandescence (LII) methods (e.g., Liati et al., 2014; Boies et al., 2015; Saffaripour et al., 2017, 2020).

An alternative possibility for the significance of sub-10 nm non-volatile particles includes the potential contributions of less volatile organic matter (as compared with $C_{40}H_{82}$) or metal compounds. Fushimi et al. (2019) showed that the mass contribution of the sum of trace elements (other than carbonaceous and sulfur compounds) was comparable to that of elemental carbon (soot) for UFP samples (~10–30 nm) collected at NRT. Saitoh et al. (2019a) reported that metal elements including Ca, Fe, Si, Mg, K, Zn, Pb, and Ni were the major compositions of these trace elements.

Lines 584-606

(26) Lns 405-407: See earlier comment about real-world vs. certification emissions measurements

Please see the answer to the comment (19).

(27) Technical corrections:

Ln 33: "supply" is an awkward use of the word here. Suggest changing "can supply" to "emit"

Ln 49: change "significant evolution" to "significant formation and evolution"

Lns 151-152: change "might act as" to "might contribute to"

Ln 197: change "accord" to "accordance"

Ln 203: change "after" to "downstream of"

Ln 216: change "required by" to "in"

Ln 218: change “required specification” to “requirements”

Ln 233: change “individual aircraft” to “individual aircraft movements”

Ln 377: change “researches” to “research”

Ln 386: change “evidences” to “evidence”

Ln 395: change “organic matters” to “organic matter”

Figure 3: This figure does not add any value to what has already been described in the text. It can be removed.

Figure 4 (a): In the legend, change “specification” to “manufacturer specification”

Figure 4 (b): In the legend, change “SAE ARP6320” to “SAE ARP6320 minimum specification”

Figure 5: delete “are shown” from figure caption

Figure 10 (a) and (b): change “Unheat” to “Unheated” in the legend and in figure

We have corrected the above points. We appreciate the referee for detailed proofreading. We have removed Fig. 3 following the referee’s comment.

References:

Beyersdorf et al., Atmos. Chem. Phys. 2014, 14, 11–23

Durdina et al., Aerosol Sci. Technol. 2016, 50, 906–918

Herndon et al., Environ. Sci. Technol. 2008, 42, 1877–1883

Maricq, Aerosol Sci. Technol. 2014, 48, 620–629

Moore et al., Sci Data 2017, 4, 170198

Lobo et al., Atmos. Environ. 2012, 61, 114–123

Timko et al., Environ. Sci. Technol. 2013, 47, 3513-3520

Trueblood et al., Atmos. Chem. Phys. 2018, 18, 17029–17045

We thank the referee for providing the information. We have added some of the references in the revised version.

# Characteristics of sub-10 nm particle emissions from in-use commercial aircraft observed at Narita International Airport

Nobuyuki Takegawa[1], Yoshiko Murashima[2], Akihiro Fushimi[3], Kentaro Misawa[1], Yuji Fujitani[3], Katsumi Saitoh[3,4], and Hiromu Sakurai[2]

[1]Department of Chemistry, Graduate School of Science, Tokyo Metropolitan University, Hachioji, Tokyo 192-0397, Japan.
[2]National Institute of Advanced Industrial Science and Technology, Tsukuba, Ibaraki 305-8563, Japan.
[3]National Institute for Environmental Studies, Tsukuba, Ibaraki 305-8506, Japan.
[4]Environmental Science Analysis and Research Laboratory, Hachimantai, Iwate 028-7302, Japan.

*Correspondence to*: Nobuyuki Takegawa (takegawa@tmu.ac.jp)

**Abstract.** ~~Civil aviation is undergoing rapid growth as a result of global economic development.~~ The ~~C~~characterization~~ing~~ of ultrafine particle emissions from jet aircraft equipped with turbofan engines, which are commonly used in civil aviation, is an important issue ~~for~~in the assessment of the impacts of aviation on climate and ~~on~~ human health. ~~Previous studies have reported that particle number emissions from jet aircraft are dominated by volatile particles (mainly sulphate and organics) with mode diameters of 10–20 nm and that non-volatile particles (mainly soot) exhibit mode diameters of ~20–60 nm, depending on the engine types and thrust conditions. However, there are significant uncertainties in measuring particles with diameters smaller than ~10 nm, especially when fresh aircraft exhaust plumes are measured near the emission sources.~~ We conducted field observations of aerosols and carbon dioxide ($CO_2$) near a runway ~~of~~at Narita International Airport, Japan, in February 2018~~,~~. We used an ultrafine condensation particle counter (UCPC) and a condensation particle counter (CPC) with unheated and 350°C heated operation modes ~~with specific focuses on~~to investigate the contributions of sub-10 nm size ranges to the total and the non-volatile particle~~s~~ number concentrations. The performance of the 350°C heated mode was tested in the laboratory to verify the consistency with existing methods for non-volatile particle measurements. We also used a scanning mobility particle sizer (SMPS) with unheated and 350°C heated modes and an engine exhaust particle sizer (EEPS) for the measurements of particle number size distributions. Spiked increases in the particle number concentrations and $CO_2$ mixing ratios were observed to be associated with ~~wind~~the directions of wind from the runway, which can be attributed to diluted aircraft exhaust plumes. We estimated the particle number emission indices (EIs) for discrete take-off plumes using the UCPC, CPC, and $CO_2$ data. ~~The median total particle number EI with diameters larger than 2.5 nm was ~60 times greater than the median non-volatile particle number EI with diameters larger than 10 nm for take-off plumes. This value can be interpreted as the difference between total particle number emissions under real-world conditions and non-volatile particle number emissions regulated by standard engine tests.~~ The median values of the total and the non-volatile particle number EIs for diameters larger than 2.5 nm as derived from the UCPC data were found to be $1.1 \times 10^{17}$ and $5.7 \times 10^{15}$ kg-fuel$^{-1}$, respectively. More than half ~~of~~ the particle number~~s in the plumes~~ EIs were ~~found~~ in the size range smaller than ~10 nm ~~on average~~ for both the total and the non-volatile particles in most of the cases analyzed in this study. The

UCPC, CPC, SMPS, and EEPS data consistently suggested that ~~T~~the mode diameters of the size distributions of the particle number EIs were ~~found to be~~ smaller than ~~~~10 nm for both the total and the non-volatile particles~~in most cases, and the peak EI values were larger than those previously reported under real world operating conditions~~. The significance of sub-10 nm size ranges for the total particles in the diluted plumes was qualitatively consistent with previous studies, but that for the non-volatile particles was unexpected. Possible factors affecting the similarities and differences compared with the previous findings are discussed.~~This study provides new insights into the significance of sub-10 nm particles in aircraft exhaust plumes under real world conditions, which is important in understanding aviation impacts on human health and also in developing aviation emission inventories for regional and global models.~~

## 1 Introduction

Civil aviation ~~is~~has grown rapidly ~~growing~~ as a result of global economic development. Consequently, the ~~environmental~~ impacts of aircraft emissions on climate and human health ~~has~~have been recognized as an important issue (ICAO, 2017; Masiol and Harrison, 2014; Stacey, 2019; and references therein). The characterization of ultrafine particles (UFPs; diameters of < 100 nm) is key to understanding the environmental impacts of aircraft emissions because the particle number and mass emissions from jet engines are often dominated by the UFP size range (Masiol and Harrison, 2014; Stacey, 2019; and references therein). ~~A unique aspect of aircraft emissions is that they can supply gaseous and particulate matter directly to the global atmosphere without any wet removal processes.~~

~~From the viewpoint of impacts on climate, t~~The primary importance of aviation-produced aerosol particles in assessing the climate impacts is the formation of contrail cirrus clouds from soot or black carbon (BC) emitted at aircraft cruising altitudes (Kärcher and Voigt, 2017; Kärcher, 2018). ~~that~~Furthermore, ~~they~~aircraft emissions can significantly affect the number concentrations of Aitken~~-~~ mode particles ~~and, potentially, the formation of clouds~~ in the upper troposphere (Wang et al., 2000; Lee et al., 2010; Righi et al., 2013, 2016). Righi et al. (2013, 2016) showed that the impacts of aviation on aerosols were sensitive to the parameterization of nucleation-mode particles (<~20 nm) in their simulation model. In our view, the contribution of aircraft emissions to the number concentration of nucleation or Aitken mode particles relative to that of other sources (new particle formation and surface emission sources) is poorly understood. ~~Specifically, soot or black carbon (BC) particles emitted from aircraft at their cruising altitudes could have a key role in the formation of contrail cirrus clouds (Kärcher and Voigt, 2017; Kärcher, 2018).~~

~~From the viewpoint of risk to human health, ultrafine particles (UFPs; diameters of <100 nm) emitted from aircraft have become a public concern, especially near airports (Masiol and Harrison, 2014; Stacey, 2019).~~ The health impacts of UFPs, although they are not specific to aircraft emissions, have been extensively studied by many researchers (Oberdörster et al., 2005; Ohlwein et al., 2019, and references therein). UFPs can be efficiently deposited ~~onto~~in the nasal, tracheobronchial, and alveolar regions in the human respiratory system, and the uptake and translocation (physical clearance) of solid UFPs such as soot into the blood and lymph circulation could be an important pathway (Oberdörster et al., 2005). Sub-10 nm particles

could be efficiently deposited in the olfactory mucosa, and the subsequent translocation of solid particles along the axons of the olfactory nerve might be a concern (Oberdörster et al., 2005). ~~Moreover,~~ A recent study suggested that the surface reactivity of aviation-induced soot particles may increase with decreasing particle size (Jonsdottir et al., 2019). However, the health impacts of UFPs emitted from aircraft have not been well established, as pointed out by Ohlwein et al. (2019).

A number of experiments have been performed at engine-test facilities and under real-world conditions to investigate gaseous and particulate emissions from aircraft equipped with turbofan engines, which are commonly used in civil aviation (e.g., Hagen et al., 1998; Petzold et al., 1999, 2005; Kärcher et al., 2000; Brock et al., 2000; Herndon et al., 2008; Westerdahl et al., 2008; Onasch et al., 2009; Kinsey, 2009; Timko et al., 2010, 2013; Lobo et al., 2015a, 2015b; Moore et al., 2017a, 2017b; Kinsey et al., 2019; Yu et al., 2017, 2019; Durdina et al., 2019). The key findings from the previous studies include the following two points. First, significant formation and evolution of volatile particles with diameters smaller than ~~~10 nm can take place during plume expansion, depending on the sulfur content of the fuel, ~~and~~ the age of the plume, and the ambient conditions (Petzold et al., 1999, 2005; Kärcher et al., 2000; Brock et al., 2000, Onasch et al., 2009; Timko et al., 2010, 2013). Second~~ly~~, non-volatile particles, which are assumed to be equivalent to soot or BC particles, primarily have sizes in the range larger than ~10 nm (geometric mean diameter (GMD) of ~20–~~5~~60 nm in particle number size distributions) under various operating conditions, with the largest GMDs under ~100% engine-thrust conditions (Petzold et al., 1999; Lobo et al., 2015a, 2015b; Moore et al., 2017a; Durdina et al., 2019). Zhang et al. (2019) recently proposed a global-scale aviation emission inventory for BC particles by integrating the existing datasets of non-volatile particle emission indices (EIs).

Alongside these scientific studies, the International Civil Aviation Organization (ICAO) has authorized a new regulatory standard for the mass and number emissions of particles emitted from aircraft engines (ICAO, 2017). In the method for measuring non-volatile particle number concentrations described in the Aerospace Recommended Practice (ARP) 6320, issued by the Society of Automotive Engineers (SAE-ARP6320) (SAE, 2018), the number concentrations of aerosol particles with diameters larger than 10 nm are measured downstream of a volatile particle remover (VPR) heated to 350°C. The SAE-ARP6320 has been developed for the certification of jet engine emissions and may not be directly compared with ambient measurement data. Some of the above-mentioned~~previous~~ studies ~~mentioned above~~ employed sampling methods equivalent to SAE-ARP6320 for field measurements of particulate emissions from in-use aircraft (Lobo et al., 2015a).

Direct measurements of UFPs behind jet engines (either in engine test cells or aircraft hangers) can provide systematic emission data as a function of the engine thrust and fuel types from selected jet engines under well-controlled conditions. A common issue in measuring UFPs behind jet engines in the previous scientific studies and in the regulatory standard is ~~that there are~~the significant loss~~es~~ of particles in ~~the~~long sampling tubes and/or the VPR when fresh aircraft exhaust plumes are sampled ~~directly behind jet engines~~ (Kinsey, 2009; Lobo et al., 2015a, 2015b; Durdina et al., 2019). Although corrections for particle loss~~es~~ have been extensively evaluated and ~~are~~ carefully considered for quantifying particle number concentrations, the absolute values of the correction factors and relative errors associated with the correction~~s~~ tend to be larger for smaller particles (Kinsey, 2009; Lobo et al., 2015a, 2015b; Durdina et al., 2019). Furthermore, the large uncertainty in measuring the

particle number size distributions ~~with~~for diameters smaller than ~~~~20 nm by using mobility size spectrometers is also of great concern (Wiedensohler et al., 2012). These technical issues should be properly considered for better characterization of aircraft exhaust particles.

Field measurements of advected (diluted) aircraft exhaust plumes near runways are not optimal for obtaining systematic emission data, whereas potential artifacts associated with long sampling lines and/or high concentrations of condensable materials can be reduced by this approach. Furthermore, a variety of exhaust plumes from different types of in-use aircraft engines can be collectively characterized by field measurements near runways. Considering that the accessibility to platforms for sampling fresh engine exhausts (engine test cells, aircraft hangers, and runways) is generally restricted, these approaches should be complementarily selected for better characterizing UFP emissions from aircraft. Consistent integration of the data is also important for constructing reliable emission inventories from the aviation sectors for the global troposphere (cruising altitudes), where the accessibility to sampling platforms is extremely limited.

We conducted field measurements of UFPs near a runway ~~of~~at Narita International Airport (NRT), Japan~~, in February 26, 2018 (Fushimi et al., 2019)~~. We used multiple instruments for the measurements of particle number concentrations and size distributions and carefully investigated the performance and consistency of these instruments. The purpose of the present study ~~is~~was to investigate the emission characteristics of sub-10 nm particles from commercial aircraft operating under real-world conditions.

## 2 Experimental

### 2.1 Field observations

The field measurements were performed ~~in~~using two containers placed at an observation point ~180 m from the cent~~r~~erline of runway A (~140 m from the edge of the runway) ~~of~~at NRT between February 5 and ~~February~~ 26, 2018 (Fushimi et al., 2019). Fig. 1 shows an approximate layout of NRT with the location of the observation point. The aerosol instruments used for the field measurements consisted of an ultrafine condensation particle counter (UCPC~~;~~, Model 3776~~;~~, TSI, Inc., Shoreview, MN, USA; $d_{50}$ = 2.5 nm), a condensation particle counter (CPC~~;~~, Model 3771~~;~~, TSI; $d_{50}$ = 10 nm), a scanning mobility particle sizer (SMPS~~;~~, Model 3080~~;~~, TSI) ~~consisting of~~equipped with a differential mobility analy~~s~~zer (long DMA~~;~~, Model 3081~~;~~, TSI) and a CPC (Model 3022A; TSI; $d_{50}$ = 7 nm), an engine exhaust particle sizer (EEPS, Model 3090~~;~~, TSI), and two sets of cascade impactor samplers (Nano MOUDI II~~;~~, Model 125B~~;~~, MSP Corp., Shoreview, MN, USA). The UCPC and CPC used for the field measurements ~~are~~were the same as those used for airborne measurements in our previous studies (Takegawa and Sakurai, 2011; Takegawa et al., 2014, 2017, 2020~~; Takegawa et al., 2017; Takegawa et al., in press~~), except for the dilution/heater sections described below. Number concentrations of aerosol particles with diameters larger than 2.5 nm or 10 nm, as measured by the UCPC or CPC, are referred to as $N_{2.5}$ or $N_{10}$, respectively. Details of the performance of the UCPC and CPC ~~will be~~are described later. The other instruments included a carbon dioxide ($CO_2$) monitor (Model LI-840~~;~~, L~~I~~i-C~~OR~~or Biosciences, Lincoln, NE, USA), a nitrogen oxides ($NO_x$) monitor (APNA-370, Horiba,

Japan), meteorological sensors, and a video camera for monitoring aircraft passages. We used the data from the UCPC, CPC, SMPS, EEPS, and $CO_2$ monitor recorded ~~from~~during February 15~~ through February~~ 22, 2018~~,~~ for the present analysis. Although $NO_x$ data are useful for characterizing aircraft emissions, we did not use those data because the response time was not sufficient ~~to~~for capture~~e~~ing rapid changes in the concentration in aircraft plumes.

Fig. 2a illustrates a schematic diagram of the sampling setup for the UCPC, CPC, SMPS, and $CO_2$ monitor. Ambient air was drawn into the container through a stainless-steel tube (ID: 10 mm; length: ~3 m) and was split into a bypass flow connecting to a piston pump and sample flows for aerosol and $CO_2$ measurements. The total flow rate through the main tube (~~the~~ sum of the bypass and sample flows) was ~20 L $min^{-1}$. The aerosol sample flow was diluted by a factor of ~5 by using particle-free air (~~~~2 L $min^{-1}$) to extend the concentration range measured by the UCPC and CPC, which would otherwise have been limited by particle-coincidence effects. The diluted sample flow was then passed through a~~n~~ stainless-steel evaporation tube (~~stainless-steel tube;~~ ID: 7.5 mm; tube length: ~~~~3~~0~~2~~0 mm; heated section: 200 mm) for heated sampling or through a bypass tube for unheated (room temperature) sampling. A thermocouple sensor was attached ~~on~~to the upstream part of the evaporation tube for ~~the~~ temperature control. The three-way valve was switched between the unheated and heated modes every 8 h. We set the heater temperature to 250°C during February 7–9, 150°C during February 11–13 and 22–23, and 350°C during February 15–21. We used the data obtained during the unheated and 350°C~~-~~ heated modes for the present analysis. The characterization of the 150 and 250°C heated modes is ~~now~~ ongoing and will be presented elsewhere. A copper tube (ID: 7.5 mm; length: ~600 mm) between the evaporation tube and the valve was used to cool the heated sample air. The sampling method for 350°C~~-~~ heated $N_{10}$ approximately correspond~~ed~~s to the ~~standard procedure~~method for measuring non-volatile particles described in SAE-ARP6320 (SAE, 2018), although we did not use a thermal denuder or a catalytic stripper so as to reduce the particle diffusion loss~~ of particles~~. The estimation of potential artifacts is described in ~~the next s~~Section 2.2. The tube downstream of the three-way valve was split into individual sample flows for the UCPC (~~~~1.4 L $min^{-1}$), CPC (~~~~1 L $min^{-1}$), and SMPS (~~~~0.3 L $min^{-1}$). Electrically conductive tubes (ID: 4.8 mm; Part 3001788, TSI) were used for the connections between the splitter and the instruments. The SMPS was disconnected from the dilution~~ and~~/heater section after February 18, and the flow rate settings were changed accordingly. Note that the flow rates ~~that were critical~~ for calculating the dilution factor were calibrated by using the standard flowmeter at the National Institute of Advanced Industrial Science and Technology (AIST). The dilution factor was estimated to be ~3.8 before February 18 and ~6.1 after that date. ~~Furthermore, t~~The residence time in the ~~heated section~~evaporation tube (320 mm, 350°C) was ~~~~0.190.15 s before February 18 and ~~~~0.210.17 s after that. These values are ~~slightly~~ shorter than the requirement for the residence time (>0.25 s) described in SAE-ARP6320 (SAE, 2018)~~-~~, although the actual temperature profile of the sample air inside the evaporation tube and its downstream was not measured. The performance of the evaporation tube was tested using tetracontane ($C_{40}H_{82}$) particles, as described in Section 2.3. After the SMPS had been disconnected, the CPC 3022 was connected directly to the main sampling tube upstream of the dilution/heater section. This permitted an overall validation of the dilution method, because the maximum concentration range of the CPC 3022 was extended to $10^7$ $cm^{-3}$ by photometric detection. Although we used the dilution method to reduce the effects of particle coincidence, we frequently observed high particle number

concentrations ~~of particles~~ (>$10^5$ $cm^{-3}$) downstream of the dilution section. The effects of particle coincidence were corrected ~~by~~ using the methods described ~~by~~in our previous studies (Takegawa and Sakurai, 2011; Takegawa et al., 2017). The correction factors were as high as ~40% at nominal (uncorrected) particle number concentrations of ~~~~5 × $10^5$ $cm^{-3}$ and ~~~~1.2 × $10^5$ $cm^{-3}$ for the UCPC and CPC, respectively. The uncertainty in the corrections would become larger at even higher concentrations.

As mentioned earlier, the measurements of particles below ~~~~20 nm ~~by~~using mobility size spectrometers might include large uncertainties (Wiedensohler et al., 2012). The major sources of uncertainties in the SMPS measurements originated from the corrections for the charging efficiency and Brownian diffusion, the latter generally being more significant for nanoparticles. The Aerosol Instrument Manager (AIM) software provides correction tools for these factors. We have found that the number size distributions at diameters below 20 nm show non-negligible differences for different versions of the software. We used ~~the~~ AIM version 9.0 for the present analysis, with the diffusion loss correction enabled~~turned on~~. The effects of the AIM diffusion correction on the derived number size distributions are described in Section S2 of the Supplement.

The EEPS was operated independently ~~with~~from the UCPC/CPC/SMPS inlet system (Fig. 2b) and it measured the unheated particle number size distributions during the entire period. The sample flow rate of the EEPS was 10 L $min^{-1}$. A copper tube (ID: 10 mm, length: ~2 m), electrically conductive tubes (ID: 4.8 and 7.9 mm; total length: ~1 m; Part 3001788, TSI), and a glass manifold (inner diameter: 40 mm; total length: 600 mm) were used for the ambient sampling. A bypass pump (flow rate: 10 L $min^{-1}$) was used to reduce the particle diffusion loss. We used the default instrument matrix for the EEPS, which may underestimate size and concentration of particles larger than ~75 nm (Wang et al., 2016). Although the particle diameter range detectable by the EEPS extended from ~6 to 5~~0~~20 nm, our laboratory experiments ~~have~~ showed~~n~~ that the EEPS may significantly underestimate particle number concentrations below ~~~~10 nm. Reduced detection efficiencies of sub-10 nm particles can also be inferred from the EEPS data obtained by other ~~investigators~~researchers (Moore et al., 2017a). The evaluation of the EEPS is ~~now~~ ongoing and will be presented elsewhere. In this study we used the EEPS data for particle diameters larger than 10 nm.

The $CO_2$ instrument was calibrated by using two $CO_2$ standards (397.2 and 1032 parts per million by volume (ppmv)) twice a day during the measurement period. The injection of the $CO_2$ standards was performed automatically by using solenoid valves. We found that the sensitivity of the instrument was generally stable during the measurement period.

The $N_{2.5}$, $N_{10}$, EEPS, and $CO_2$ data were obtained every 1 s, and the SMPS data for particle diameters from 15 to 660 nm were obtained every 5 min (scanning time: 3 min). When we observed spiked increases in the particle number concentrations and $CO_2$ mixing ratios in aircraft plumes, the timing of the detection of the concentration peaks did not exactly match ~~among~~between the individual instruments. Because this was likely caused by differences in the response time of the instruments and the delay time in the sampling tubes, the data was shifted accordingly (<~~~~10s).

The overall penetration efficiencies of particles through the sampling tubes were estimated by using the theoretical formulae proposed by Gormley and Kennedy (1949). Details of the calculation procedures are given in Section S1 of the

Supplement. The penetration efficiency for the UCPC and CPC sampling line (unheated mode; from the top of the inlet to the flow splitter) was estimated to be 70%, 87% and 94% for particle diameters of 5, 10, and 20 nm, respectively. The penetration efficiency through the evaporation tube and the detection efficiencies of the UCPC and CPC are important parameters for the data interpretation and are discussed in detail in Section 3.1. The penetration efficiency for the SMPS sampling line (unheated mode; from the top of the inlet to the SMPS) was estimated to be 79% and 85% for 15 and 20 nm, respectively, and that for the EEPS sampling line (from the top of the inlet to the EEPS) was estimated to be 94% and 98% for 10 and 20 nm, respectively.

The particle diffusion loss during sampling is an important issue for the quantification of UFPs, as mentioned in Section 1. The corrections for the penetration efficiencies through the sampling tubes and the detection efficiencies (see Section 3.1 for details) were not incorporated in the UCPC and CPC data presented in Sections 3.2.1–3.2.4 because the actual size distributions in the sub-10 nm size range were uncertain. Furthermore, the corrections for the penetration efficiencies were not incorporated in the SMPS and EEPS data presented in Sections 3.2.2–3.2.3 for consistency with the UCPC/CPC data: i.e., they include only the default (internal) corrections for the individual instruments. We considered the effects of particle diffusion loss as systematic uncertainties. We also considered the penetration efficiencies through the sampling tubes and the detection efficiencies for estimating the size distributions of particle number EIs in Sections 3.2.5 and 4.

### 2.2 Potential artifacts

Potential artifacts due to the nucleation ~~and growth~~ of ~~vaporized~~gaseous compounds vaporized from particles ~~after~~in the evaporation tube (hereafter referred to as nucleation artifacts) ~~are~~were evaluated. Predicting the nucleation rates requires an estimate of the supersaturation of nucleating compounds, which is highly uncertain. Here we evaluate the growth rate of nucleated clusters under ~~a~~the given condition. The upper limit of this effect can be estimated by assuming that the number concentration of the vaporized compounds remains constant after a certain period of time (~1 s) and that all ~~of~~ the compounds are condensed ~~o~~into nucleated clusters (e.g., sul~~ph~~furic acid). In real situations, only a small fraction of the vaporized compounds might ~~act as~~contribute to the condensational growth of particles because of possible increases in their saturation vapo~~u~~r pressures by thermal decompositions and their deposition onto the inner surface of the sampling tube.

Let us assume a condensable material (number concentration of molecules: $c$; molecular weight: $MW$) in the gas-phase vaporized from particles. The original mass concentration in the particle phase before heating, $m$, is expressed as follows:

$$m = \frac{MW}{N_A} c \qquad (1)$$

where $N_A$ is the Avogadro number. Assuming a kinetic regime, the growth of nucleated particles is governed by the following expression (Seinfeld and Pandis, 2006):

$$\frac{\pi}{2}\rho D_p^2 \frac{dD_p}{dt} = \frac{MW}{N_A}\frac{\pi}{4} D_p^2 \bar{v}\alpha(c - c_{eq}) \qquad (2)$$

where $\rho$ is the particle density, $D_p$ is the diameter of nucleated particles, $\bar{v}$ is the mean thermal velocity of condensable gas molecules, $\alpha$ is the accommodation coefficient, and $c_{eq}$ is the equilibrium number concentration. Assuming $\alpha = 1$ and $c_{eq} = 0$ (maximum molecular flux), we obtain the~~is~~ expression:

$$\frac{dD_p}{dt} = \frac{\bar{v}}{2\rho} m \qquad (3)$$

If we consider sulfuric acid as a condensable material, $dD_p/dt$ (m $s^{-1}$) can be approximated as $0.1m$ at 350°C (~~the~~ maximum gas temperature), where $m$ is expressed in units of kg $m^{-3}$. The residence time for particle growth after the evaporation tube is estimated to be <1 s. The residence time of 1 s and the dilution factor of 5 lead to ~~an~~the estimation~~e~~ that the maximum particle growth is 1 nm at an ambient mass concentration of 50 µg $m^{-3}$. The minimum particle diameter at which the detection efficiency becomes zero ~~are~~is ~2 and ~7 nm for the UCPC and CPC, respectively (Takegawa and Sakurai, 2011; Takegawa et al., 2017). If we assume an initial cluster size of 1 nm (approximately the critical cluster size of sulfuric acid), the effects of the artifacts on $N_{2.5}$ would be significant in aircraft exhaust plumes with relatively high concentrations (>~~–~~50 µg $m^{-3}$), and those on $N_{10}$ (and SMPS) would be significant at very high concentrations (>~~–~~300 µg $m^{-3}$). This estimation~~e~~ does not change significantly if we assume high-molecular-weight organic compounds from jet~~-~~ engine lubrication oil (slower thermal velocities and smaller particle densities compared with sulfuric acid).

Other potential artifacts may originate from the condensational growth of non-volatile particles (or residual particles downstream of the evaporation tube) smaller than the detectable size range of the UCPC (diameter < 2 nm). For example, residual particles with diameters of ~2 nm may grow to ~3 nm at an ambient mass concentration of 50 µg $m^{-3}$. However, this effect is significant only in the presence of a large fraction of non-volatile particles with diameters below 2 nm.

### 2.3 Laboratory experiments

The accuracy of the measurements of particle number concentrations was the key issue in this study and th~~i~~us was evaluated in the laboratory at AIST before and after the field measurements. We mainly used the data obtained after the field measurements because they were more comprehensive than those obtained before the measurements. The test items included the size-resolved detection efficiencies of the UCPC and CPC, the penetration efficiency of non-volatile particles through the dilution/heater section, and the removal efficiency of volatile compounds through the evaporation tube.

An electrospray aerosol generator (EAG~~;~~; Model 3480~~;~~, TSI), a combustion aerosol standard (CAST; Matter Engineering, AG, Wohlen, Switzerland) with a tube furnace for thermal treatment at 350°C, and a custom-made tube furnace for supplying ~~of~~ condensable vapo~~u~~rs were used to generate polydisperse aerosol particles for the calibrations. We used

sucrose particles supplied from the EAG (particle diameter range: 6–15 nm) for the detection efficiency experiment, non-volatile propane soot particles supplied from the CAST (15–100 nm) for the penetration efficiency experiment, and ~~tetracontane (~~$C_{40}H_{82}$~~)~~ particles supplied from the tube furnace particle generator (15–30 nm) for the removal efficiency experiment. The tube furnace downstream of the CAST was used to remove organic compounds internally or externally mixed with soot. We used a volatility tandem DMA with a heater temperature of 350°C to confirm that the thermal treatment efficiently removed organic compounds; i.e., there was no significant difference in the mobility diameter of soot particles between the two DMAs.

The experimental apparatus for measuring the size-resolved detection efficiencies of the UCPC and CPC was similar to that~~ose~~ used in our previous studies (Takegawa and Sakurai, 2011; Takegawa et al., 2017), except that the sampling line~~s were~~was ~~somewhat~~ longer for the CPC. The length~~s~~ of the sampling line~~s~~ for the CPC was ~90 cm, ~~were~~which was limited by the instrument layout in the observation rack. ~~Fig. 3 shows the experimental apparatus for testing the penetration and removal efficiencies.~~ We set the particle diameters at 15, 30, 50, and 100 nm for testing the penetration efficiencies~~y~~ and at 15 and 30 nm for testing the removal efficiencies, in accordance with the SAE-ARP6320 protocol. The flow rate through the evaporation tube was set at 2.4 L $min^{-1}$. We used an aerosol electrometer (AE~~;~~, Model 3068B~~;~~, TSI) and a reference CPC (ref CPC~~;~~ Model 3775~~;~~ TSI) as reference instruments. ~~-~~These were calibrated with the standard AE maintained by AIST for particle number concentrations at ambient pressures in the size range of 10–300 nm.

We also tested the removal efficiencies~~y~~ of $C_{40}H_{82}$ particles for diameters of 30 and 50 nm in the laboratory at Tokyo Metropolitan University (TMU)~~using a similar experimental setup as shown in Fig. 3~~. We used another CPC (Model 3772; TSI), which is essentially the same as ~~a~~ CPC Model 3771, for the detection of residual particles ~~after~~downstream of the evaporation tube because the conditions for the CPC 3771 were not optimized during the experiments at TMU. ~~An additional pump was used to maintain a~~ The flow rate ~~of~~through the evaporation tube was set at either 2.4 or ~~-~~2.7 L $min^{-1}$ ~~through the evaporation tube.~~ to test the dependency of the removal efficiencies on the flow rate. Considering that the polydisperse size distributions of the $C_{40}H_{82}$ particles generated at TMU were rather broad, we also measured the removal efficiencies of doubly charged particles (43 nm for 30 nm and 72 nm for 50 nm).

## 3 Results

### 3.1 Laboratory experiments

Fig. ~~4~~3a shows the size-resolved detection efficiencies of the UCPC and CPC measured at AIST. The detection efficiencies for the UCPC and CPC were empirically estimated by using our previous calibration results for the CPC (Takegawa and Sakurai, 2011), the manufacturer~~'s~~ specifications for the UCPC (Takegawa et al., 2017), and the penetration efficiencies in the instrument (for the UCPC; Wimmer et al. (2013)) and the sampling lines. The penetration efficiencies were calculated by using the theoretical formulae proposed by Gormley and Kennedy (1949). Further details of the

empirically estimated detection efficiencies are given in Fig. S1 in the Supplement. We found a good agreement between the experimental data and the estimated detection efficiencies for both the UCPC and CPC.

Fig. 43b shows the penetration and detection efficiencies~~y~~ of non-volatile soot particles through the 350°C~~-~~ heated~~-~~ mode sampling tubes as measured by the UCPC. The temperature was set at room temperature (~19–21°C) and ~~to~~at 350°C for comparison. The penetration and detection efficiencies~~y~~ include~~s~~ the penetration efficiency through the dilution/heater section and the detection efficiency of the UCPC shown in Fig. 43a. Based on the specifications ~~required by~~in the SAE-ARP6320 protocol, the penetration efficiency through a VPR should be ~~higher than or~~ equal to or higher than 30, 55, 65, or 70% for particle diameters of 15, 30, 50, and 100 nm, respectively. Our data showed that the penetration efficiency was well above the required~~d~~ments ~~specification~~ for all diameters tested. ~~Because a~~It was rather difficult to perform a simple theoretical prediction of the penetration efficiency at 350°C ~~is not straightforward,~~ because the actual temperature profile of the sample air was uncertain. Therefore, ~~we scaled the penetration efficiency curve at room temperature to match the values observed at 350°C for larger diameters (30, 50, and 100 nm).~~ the penetration efficiency curve at 350°C (not shown in Fig. 3) was determined by scaling the calculated curve at 20°C with the experimental values at 350°C and at room temperature for larger diameters (>30, 50, and 100 nm).

The SAE-ARP6320 protocol specifies that the removal efficiencies of $C_{40}H_{82}$ particles in a VPR should be higher than 99.9% for particle diameters of 15 and 30 nm. For the removal efficiency test at AIST, we confirmed that the removal efficiencies of $C_{40}H_{82}$ particles for diameters of 15 and 30 nm were >99.9% (remaining fraction of <0.1%) ~~(~~for both ~~by~~ the UCPC and CPC~~) and that for 50 nm was >99% (by the CPC 3772)~~. For the removal efficiency test at TMU, we first confirmed that there was no significant difference exceeding the experimental uncertainties between the two flow rate settings (2.4 and 2.7 L $min^{-1}$) for both the UCPC and CPC, and we mainly used the results for 2.7 L $min^{-1}$ (shorter residence time). Table 1 presents the experimental results. The remaining fractions for 30 nm particles were found to be 0.3 (+0.2/–0.0) % and <0.1% for the UCPC and CPC, respectively. The difference between the results from the AIST and TMU experiments for the UCPC was not well identified, and we took the results from the TMU experiments for conservative estimates. The remaining fractions for 50 nm particles were found to be 5 (+4/–1) % and <0.1% for the UCPC and CPC, respectively. The remaining fraction for 73 nm was not quantified because of low particle number concentrations (thus the multiple-charge correction for 50 nm was minor). These results suggested that about 5% of the 50 nm $C_{40}H_{82}$ particles might not have fully vaporized but shrunk to sizes between 2.5 and 10 nm downstream of the evaporation tube. Potential influences on the interpretation of the ambient data are discussed later~~Although there are uncertainties in the actual gas temperature inside the evaporation tube, the removal efficiencies of $C_{40}H_{82}$ particles in our system are found to be comparable to those required by the SAE-ARP-6320 protocol.~~

### 3.2 Field observations

#### 3.2.1 Particle number concentrations

Fig. ~~5~~4 shows time series of $N_{2.5}$ and $CO_2$ obtained on February 15, 2018. The inlet valve was switched from the unheated to the 350°C- heated mode at 16:00 local time (LT). The wind directions were east or east-southeast for Fig. ~~5~~4a (average ± standard deviation (1σ) of the wind speeds were 3.9 ± 0.7 m $s^{-1}$) and east or east-northeast for Fig. ~~5~~4b (average ± 1σ of the wind speeds were 4.3 ± 0.6 m $s^{-1}$), indicating that ~~(i.e., the~~relatively stable winds ~~were~~ from the direction of the runway~~)~~ were dominant. The ambient temperature was ~10°C for Fig. ~~5~~4a and ~8°C for Fig. ~~5~~4b. We did not observe a significant enhancement of aerosols or $CO_2$ when the air parcels originated from the opposite direction from the runway during aircraft operating times (06:00-23:00 LT). The spikes in the concentrations of aerosol particles and in $CO_2$ mixing ratios shown in Fig. ~~5~~4 can be interpreted as resulting from diluted exhaust plumes from individual aircraft movements. The observed values of $N_{2.5}$ (and $N_{10}$) for the 350°C- heated mode (Fig. ~~5~~4b) were significantly lower than those for the unheated mode (Fig. ~~5~~4a) when ~~we~~ comparing~~e~~ plumes with similar enhancement levels of $CO_2$. The depletions of $N_{2.5}$ (and $N_{10}$) for the 350°C- heated mode were much larger than those expected from the difference in the penetration efficiencies~~y~~ of aerosol particles between the unheated and the 350°C- heated modes (see Fig. ~~4~~3)~~,~~. Although the characteristics of the plumes shown in Figs. 4a and 4b cannot be directly compared, the similarity in the wind conditions suggests that the ages of the plumes were comparable (~50 s). ~~suggesting~~These results imply that most of the aerosol particles in the observed plumes were volatile. We have previously shown that jet- engine lubrication oil was the major source of aerosol particles with diameters ranging from ~10 to 30 nm in air parcels observed during the measurement period (Fushimi et al., 2019). A key point in Fig. ~~5~~4 is that the number fraction of particles with diameters ranging from 2.5 to 10 nm (red area) was generally larger than that of particles with sizes above 10 nm (gra~~e~~y area), for both the unheated and 350°C- heated modes. The significance of sub-10 nm size ranges for the total particles in diluted plumes ($10^1$–$10^2$ m from the jet engines) ~~is~~was qualitatively consistent with the findings from previous studies conducted on the ground (e.g., Petzold et al., 2005; Lobo et al., 2012, 2015b) or in-flight at cruise altitudes (Petzold et al., 1999; Kärcher et al., 2000; Brock et al., 2000), but that for non-volatile particles found in this study ~~is~~was unexpected.

Fig. ~~6~~5a is a scatterplot of 1 s averaged values of $N_{10}$ versus those of $N_{2.5}$ for the 350°C- heated mode for the time period from 17:00 to 23:00 on February 15, 2018, the same data as used in Fig. ~~5~~4b. Data obtained on February 21, 2018 at slightly different flow rate settings (see ~~s~~Section 2.1) are also plotted to show the reproducibility of the results. The 1:1 correspondence line ($N_{10}$ = $N_{2.5}$) represents the state in which all particles are included in the size range larger than 10 nm, and deviations below the 1:1 line indicate ~~that~~an increase in the fractions of sub-10 nm particles ~~increase~~. These results show that many data points lie below the 1:2 line (sub-10 nm fraction of >50%) when $N_{2.5}$ exceeds ~~~~$10^5$ $cm^{-3}$. This point is more quantitatively found in the median values for each concentration bin (Fig. 5b). ~~Specifically, s~~Some data points in Fig. 5a were found on the 1:10 correspondence line (sub-10 nm fraction of ~~~~90%). The deviations from the 1:1 line would have been even larger had we considered the size-dependent loss of particles in the sampling line shown in Fig. ~~4~~3.

### 3.2.2 Size distributions of total particles

Fig. ~~7~~6 shows time series of total particle number concentrations measured by the CPC and EEPS and the particle number and volume size distributions ($dN/d\log D$ and $dV/d\log D$) ~~as~~ measured simultaneously by the EEPS and unheated SMPS for selected time periods on February 15, 2018. The total particle number concentrations measured by the CPC ($d_{50}$ = 10 nm) and EEPS (10–520 nm) showed reasonable agreement, which confirms the overall consistency between these two independent measurements. The time periods were carefully selected ~~carefully to~~for investigating~~e~~ the effects of rapid changes in the particle number concentration during each SMPS scan on the derived particle size distribution. The SMPS needed ~30 s to scan the major population of particle number concentrations in the aircraft plumes (<30 nm). Considering possible delays in the detection timing due to the residence time in the SMPS sampling tubes (<5 s), the EEPS data were averaged over 40 s around the timing of the SMPS scan corresponding to the diameter range of 15–30 nm (i.e., averaged from 10 s before to 30 s after the onset of each SMPS scan). For the SMPS scan at 14:10 LT, the particle number concentration varied by a factor of ~2 during the first 30- s scan time, but there was no systematic increase or decrease in the particle number concentration. We ~~have~~ found a reasonable agreement between the EEPS and SMPS (within a factor of ~2). For the SMPS scan at 14:20 LT, the particle number concentration decreased significantly during the 30- s scan time~~,~~ and then started to increase rapidly afterwards. The resultant number size distribution was likely affected by these concentration changes. These results demonstrate that the SMPS data can be used to investigate the characteristics of particle size distributions within specific size ranges by selecting the appropriate time windows. Note that the SMPS data tend to exhibit higher concentrations (by a factor of ~2) at smaller diameters (<20 nm) compared with the EEPS data in both cases. The difference cannot be explained by the uncertainty due to the penetration efficiencies through the sampling tube (as indicated by error bars in Fig. 6b). The difference may be due to uncertainties in the default (internal) correction algorithms in the SMPS (see Fig. S2 in the Supplement). Nevertheless, the overall size dependency (i.e., increasing particle number concentrations with decreasing particle diameters below 20 nm) is consistent between the SMPS and EEPS data.

In the enhancement events at 14:10 and 14:20 LT in Fig. ~~7~~6, the EEPS data indicate that the particle number size distribution functions below ~50 nm showed significant increases compared with that in the non-enhancement event (14:00 LT). The particle volume size distribution function below ~50 nm exhibited moderate increases in the enhancement events, but the total integrated particle volume concentrations were largely affected by accumulation-mode particles (>50 nm) in the background air. A similar feature was also found for other time periods (Fushimi et al., 2019; Misawa et al., manuscript in preparation).

### 3.2.3 Size distributions of non-volatile particles

Fig. ~~8~~7 shows the particle number and volume size distributions ~~as~~ measured simultaneously by the EEPS and the 350°C- heated SMPS for selected time periods with and without enhancements of aerosol particle number concentrations on February 15, 2018. The time periods were selected so that there ~~was~~would be no systematic increase or decrease in the

particle number concentrations during the first 30- s scan time of the SMPS. Similarly to Fig. 76, the particle number size distribution functions below ~50 nm in the enhancement events showed significant increases compared withto thatthose in the non-enhancement event for both the EEPS and the 350°C- heated SMPS. The particle number size distribution functions below ~50 nm measured by the 350°C- heated SMPS were smaller by more than an order of magnitude thancompared to those measured by the EEPS, indicating that the aircraft exhaust particles were mostly volatile below ~50 nm. Although we did not test the removal efficiency of particles with diameters larger than 50 nm, Our laboratory experiments suggest that there might remain residues of >50-nm particles in the sub-10 nm size range after the evaporation tube (the remaining fraction was ~5% for 50 nm $C_{40}H_{82}$ particles). "residues" of larger particles (>50 nm) after the evaporation tube However, they were likely negligible compared with the observed sub-10 nm non-volatile particles because the particle number concentrations for a diameter range of >50 nm measured by the EEPS (unheated) were far below the observed values of the 350°C- heated $N_{2.5} - N_{10}$ (Fig. 87a). In addition, residues of 30–50 nm particles in the sub-10 nm size range after the evaporation tube were likely minor compared with the observed sub-10 nm non-volatile particles considering the sharp decrease in the $dN/d\log D$ values from 30 to 50 nm as measured by the EEPS (the remaining fractions were ~0.3% and 2% for 30 and 43 nm $C_{40}H_{82}$ particles, respectively).

The Eeffects of nucleation artifacts (sSection 2.2) might be a major concern but were likely small under the observation conditions because the mass concentrations of aerosol particles in the aircraft plumes inferred from Fig. 87 were much lower than the threshold concentration (~50 μg $m^{-3}$) described in sSection 2.2. In fact, we did not find any systematic increases in the $N_{2.5}/N_{10}$ ratios for the 350°C- heated mode with increasing total particle volume concentrations derived from the EEPS (not shown). Furthermore, the particle number and volume size distributions derived from the 350°C- heated SMPS (Figs. 87b- and c) exhibited no indication of the presence of artificial nucleationan additional mode resulting from nucleation artifacts (Section 2.2). The 350°C heated $dN/d\log D$ functions in Fig. 87b exhibited gradual increasing trends with decreasing particle diameters from ~100 to ~15 nm., which This feature is unlikely to be explained by nucleation artifactsthe artificial growth of particles downstream of the evaporation tube because the mass concentrations of aerosols in the plumes would not have been sufficient to yield particle growth exceeding 1 nm (Section 2.2).

### 3.2.4 Particle emission indices for take-off plumes

The temporal variations and number size distributions of aerosol particles clearly indicate that the observed air parcels were significantly affected by aircraft emissions under appropriate wind conditions. However, aircraft emissions from various cycles of take-off, landing, and idling may have been mixed in the atmosphere. We calculated the enhancements of $N_{2.5}$, $N_{10}$, and $CO_2$ above the background levels (referred to as $\Delta N_{2.5}$, $\Delta N_{10}$, and $\Delta CO_2$, respectively), and extracted discrete plumes during the take-off phases by setting some criteria for these parameters (for details, see sSection S13 and Figs. S13–S35 in the Supplement for details). By using the data obtained on February 15, 16, 20, 21, and 22, we identified 132 discrete plumes for the unheated mode and 63 for the 350°C- heated mode. Particle number and volume size distributions ($dN/d\log D$

and $dV/d\log D$) for the take-off plumes were derived from the EEPS data (unheated conditions), and the enhancements of $dN/d\log D$ and $dV/d\log D$ above the background levels were calculated using the same method as for $\Delta N_{2.5}$.

The $\Delta N_{2.5}/\Delta CO_2$ and $\Delta N_{10}/\Delta CO_2$ ratios were converted into particle number EIs by assuming a $CO_2$ EI value of 3160 g of $CO_2$ per kilogram of fuel (Moore et al., 2007a; see Table ~~1~~2). The ~~C~~corrections for the penetration and detection efficiencies of the UCPC and CPC were not incorporated into the above estimates because the actual size distributions were uncertain; these values should therefore be regarded as lower limits. This point is further discussed in Section 4.1. The arrival time of the plumes was estimated to be ~30–120 s by considering the wind directions and speeds, corresponding to the transport distance of ~180–370 m from the engine exits to the observation point (Section S3 of the Supplement). We did not find a systematic dependence of the $\Delta N_{10}/\Delta CO_2$ and $\Delta N_{2.5}/\Delta CO_2$ ratios on the estimated arrival time of the plumes (~~see~~ Fig. S~~3~~5 in the Supplement), suggesting that the variation ~~of~~in plume ages did not yield significant biases in our results. We did not perform a detailed classification of the plumes by jet engine types because information on the engines of the aircraft observed at NRT was not available. We performed a simple classification of the plumes by aircraft model~~s~~ (~~see~~ Table S~~1~~2 in the Supplement), but did not find significant differences ~~among~~between the different types of aircraft.

~~The median total EI($N_{2.5}$) was ~ 60 times larger than the median non-volatile EI($N_{10}$). This value can be interpreted as the difference between total particle number emissions under real world conditions and non-volatile particle number emissions regulated by standard engine tests (SAE, 2018). Although the fact that particle emissions under real world conditions are larger than those measured during standard engine tests is well known, few studies have reported quantitative estimates of the difference.~~ The median total and non-volatile EI($N_{2.5}$) values, which likely cover the major size range of the aircraft emissions, were found to be $1.1 \times 10^{17}$ and $5.7 \times 10^{15}$ kg-fuel$^{-1}$, respectively. The difference in these values (a factor of ~20) is interpreted as the average contribution of volatile particles.

We defined the sub-10 nm fraction as $1 - \Delta N_{10}/\Delta N_{2.5}$ for the identified discrete plumes. The median and the central 50 percentile range of the sub-10 nm fraction for the unheated mode were found to be 0.63 and 0.53–0.70, respectively, and those for the 350°C- heated mode were 0.54 and 0.44–0.72, respectively (Table ~~1~~2). The significance of sub-10 nm particles for the total and the non-volatile particles, which was shown in ~~s~~Sections 3.2.1–3.2.3 (Figs. ~~5~~4–~~8~~7) as a case study, was also found in the statistical analysis of the take-off plumes. Considering that the penetration efficiencies of particles through the sampling tubes (Fig. S1 in the Supplement) and the evaporation tube (Fig. 3) tended to decrease with decreasing particle diameters below 10 nm, these results suggest that more than half the total and the non-volatile particle number EIs in the aircraft take-off plumes were found in the size range smaller than 10 nm in most cases.

Previous studies have shown that the particle number EIs can vary significantly depending on the engine type, the engine thrust, the fuel sulfur content, the plume age, and the ambient conditions (Petzold et al., 1999, 2005; Kärcher et al., 2000; Brock et al., 2000; Onasch et al., 2009; Timko et al., 2010). The sampling setup (deployed instruments and sampling location relative to the runways) and the analysis procedures (discrete plume analysis) of this study are similar to those of Lobo et al. (2012, 2015b) and Moore et al. (2017a). Therefore, it is worthwhile discussing the similarities and differences between those studies and our results. The fuel sulfur content is an important parameter for the comparison with other studies.

We do not have information on the sulfur content of the fuel that was actually used at NRT. Instead, we analyzed fuel samples (Jet A-1) provided by a jet fuel company in Tokyo (Ishinokoyu, Co. Ltd.) (Saitoh et al., 2019b). We obtained a total of five samples between August 2017 and August 2018. The sulfur content of the fuel samples ranged from 30.4 to 440 parts per million by weight (ppmw). We assume that these values are representative of the sulfur content of jet fuels commercially available in Tokyo during the observation period.

Lobo et al. (2012) reported particle number and mass EIs measured 100–350 m downwind of the runways at Oakland International Airport in August 2005. They used a fast particulate spectrometer (DMS500, Cambustion) to measure the particle number size distributions for diameters ranging from 5 to 1000 nm. The total particle number EIs for various types of engines under take-off conditions ranged from $4 \times 10^{15}$ to $2 \times 10^{17}$ kg-fuel$^{-1}$, which inclusively covered the 25–75 percentile range of the total EI($N_{2.5}$) from our measurements. The fuel sulfur content was estimated to be 240–395 ppmw.

Lobo et al. (2015b) reported the particle number and mass EIs measured near the jet engine exits and 100–350 m downwind of the runways at Hartsfield-Jackson Atlanta International Airport in September 2004. The former corresponds to the non-volatile particle EIs and the latter corresponds to the total particle EIs. They used a ~~fast particulate spectrometer (~~DMS500~~, Cambustion)~~ to measure the particle number size distributions~~ with diameters ranging from 5 to 1000 nm~~. The non-volatile particle number EIs for a JT8D-219 engine were ~1 × $10^{16}$ kg-fuel$^{-1}$ under 85% and 100% thrust conditions, which were close to the 75 percentile value of the non-volatile EI($N_{2.5}$) from our measurements. ~~Based on Fig. 7 of Lobo et al. (2015b), the medians of~~The total particle number EIs for various types of engines under take-off conditions ranged from ~~5~~7 × $10^{16}$~~5~~ to ~~3~~9 × $10^{17}$ kg-fuel$^{-1}$, which again inclusively covered the 25–75 percentile range of the total EI($N_{2.5}$) from our measurements. The information on the fuel sulfur content was not provided.

Moore et al. (2017a) reported the particle number and volume EIs for take-off plumes ~~based on field observations~~ measured 400 m downwind of the runway at Los Angeles International Airport (LAX) in May 2014~~, and provided useful dataset that can be directly compared with our results~~. They used a CPC 3775 ($d_{50}$ = 4 nm) for the measurements of total particles, a CPC 3022A ($d_{50}$ = 7 nm) for non-volatile particles, and an EEPS for the measurements of size distributions. We calculated ~~T~~the median values (and the 25–75 percentile range) of the total and the non-volatile particle number EIs provided by Moore et al. (2017a) ~~listed in Table 4 of Moore et al. (2017a) were calculated~~ to be ~~3.4~~4.6 (3.1–5.8) × $10^{16}$ and ~~1.9~~2.1 (1.1–3.6) × $10^{15}$ kg-fuel$^{-1}$, respectively~~which were comparable to the median values of the total and non-volatile EI($N_{10}$) from our measurements~~. The median and 25–75 percentile range of the total and the non-volatile EI($N_{10}$) from our measurements showed good agreement with those from Moore et al. (2017a). Although Moore et al. (2017a) used different types of CPCs, the detection efficiency curves for the CPC 3771 and 3022A were likely similar according to the manufacturer specifications. Furthermore, the EEPS data from Moore et al. (2017a) showed that the contributions from sub-10 nm particles to the total particle number EIs were relatively small (see Section 3.2.5 for details). Therefore, the good agreement between their results and the EI($N_{10}$) values from our measurements would be reasonable. The sulfur content of the jet fuel samples collected at LAX ranged from 620 to 1,780 ppmw (average value of 1,180 ppm).

Timko (2010) showed that the total particle number EIs in moderately diluted plumes (measured by a CPC 3022A), which were dominated by volatile particles, exhibited a relatively weak dependence on the fuel sulfur content (<1,500 ppmw) under high thrust conditions for various types of engines. Provided that the fuel sulfur content was likely below ~1,500 ppmw for the previous studies (Lobo et al., 2012, 2015b; Moore et al., 2017a) and this study, it might not be the major factor affecting the variability in the emissions of volatile particles among these studies (at least for diameters larger than ~10 nm). ~~Zhang et al. (2019) reported an average non-volatile particle number EI (diameter >10 nm) of $6.06\times10^{14}$ kg-fuel$^{-1}$ for various conditions of engine thrust. The average value from Zhang et al. (2019) is significantly smaller than the median non-volatile particle number EIs from Moore et al. (2017a) and from our measurements. The median non-volatile EI($N_{2.5}$) from our measurements, which may inclusively cover the size range relevant to aircraft emissions, is larger by nearly an order of magnitude than the non-volatile particle number EIs reported by Zhang et al. (2019).~~

### 3.2.5 Size distributions of total particles for take-off plumes

The enhancements of $dN/d\log D$ and $dV/d\log D$ above the background levels derived from the EEPS data were converted to the corresponding EI values ($d\mathrm{EI}(N)/d\log D$ and $d\mathrm{EI}(V)/d\log D$). As described in Section 2.1, the corrections for the penetration efficiencies through the sampling tubes (Fig. S1) were considered for the data conversion. Fig. ~~9~~8 shows the ~~size distributions of total particle number and volume EIs~~derived $d\mathrm{EI}(N)/d\log D$ and $d\mathrm{EI}(V)/d\log D$ values for the take-off plumes. ~~It should be noted that the quality of data at larger particle diameters (>~100 nm) was not sufficient because they were significantly affected by accumulation mode particles in background air.~~ The size distributions of the particle number and volume EIs for the take-off plumes observed at LAX (Moore et al., 2017a), which are characterized by bimodal log-normal distributions (nucleation and soot modes), are shown for comparison. ~~The mode diameters of $d\mathrm{EI}(N)/d\log D$ for nucleation mode reported by Moore et al. (2017a) ranged from ~10 to 20 nm. Fig. 9 suggests that the mode diameters of $d\mathrm{EI}(N)/d\log D$ for nucleation-mode particles obtained in this study were smaller than ~10 nm, and that the peak values of $d\mathrm{EI}(N)/d\log D$ were larger than those reported by Moore et al. (2017a).~~

Other previous studies also reported that aircraft emissions can be characterized by distinct bimodal size distributions ~~the mode diameters of particle number EIs generally ranged from ~10 to 20 nm~~ under high engine thrust conditions (e.g., Kinsey, 2009; Lobo et al., 2012, 2015b; Yu et al., 2017, 2019).

The total and non-volatile particle number EIs derived from the UCPC and CPC fell in the same range as those from the previous studies for take-off plumes under real-world operating conditions (Lobo et al., 2012, 2015b; Moore et al., 2017a), as described in Section 3.2.4. However, the characteristics of the size distributions appeared to be significantly different. The mode diameters of the $d\mathrm{EI}(N)/d\log D$ for the nucleation mode reported by the previous studies were 10–20 nm in most cases. We compared the $d\mathrm{EI}(N)/d\log D$ values between each size bin (midpoint diameters of 10.8, 12.4, 14.3, … nm) for the individual take-off plumes shown in Fig. 8. We found that the $d\mathrm{EI}(N)/d\log D$ at 10.8 nm exhibited the highest value for ~98% of the plumes. We also found that the $d\mathrm{EI}(N)/d\log D$ at 10.8 nm was more than two times larger than that at 14.3 nm for 79% of the plumes. These results suggest that the $d\mathrm{EI}(N)/d\log D$ values tended to increase with decreasing particle diameters

around 10–20 nm and that the mode diameters of the $d\mathrm{EI}(N)/d\log D$ for the nucleation mode were smaller than 10 nm for the majority of the plumes observed in this study. Our results also suggest that the peak values of the $d\mathrm{EI}(N)/d\log D$ for the nucleation mode were much larger than those reported by Moore et al. (2017a), in which the contributions from the sub-10 nm size range to the total particle number EI size distributions were relatively small.

The uncertainties in the $d\mathrm{EI}(N)/d\log D$ and $d\mathrm{EI}(V)/d\log D$ values at larger particle diameters (>100 nm) were considerably large in our data because they were significantly affected by the accumulation-mode particles in the background air, and also because the default instrument matrix of the EEPS might underestimate size and concentrations of particles larger than ~75 nm (Wang et al., 2016). Nevertheless, it is likely that the non-volatile particle number and volume EIs originating from soot-mode particles (>20 nm) were much smaller than those reported by the previous studies (Lobo et al., 2012, 2015b; Moore et al., 2017a). A correction for the EEPS size bin by a scaling factor of 1.1, as was done by Moore et al. (2017a), would increase the particle volume concentrations by a factor of 1.33, which does not fill the gap between the previous studies and our results. ~~An exception is Kinsey et al. (2019), who investigated the emission characteristics of a commercial gas turbine engine (CFM56-2C1) onboard a DC-8 with blending two types of fuels (military JP-8 and Fischer-Tropsch: FT) under various thrust conditions and ambient temperatures. The sulphur content of fuels for the FT fuels were much lower than that for the JP-8 fuels. They found that the mode diameters of $d\mathrm{EI}(N)/d\log D$ under high engine thrust exhibited strong dependence on the fuel composition and weak dependence on ambient temperatures. They observed mode diameters of <10 nm under high thrust conditions with the use of FT fuels, although the peak values of $d\mathrm{EI}(N)/d\log D$ (~$10^{16}$ $\mathrm{cm^{-3}}$ kg fuel$^{-1}$) were far lower than those found in this study.~~

## 4 Discussion

### 4.1 Estimates of particle number EI size distributions for take-off plumes

We estimated the possible particle number size distributions for the total and the non-volatile particles constrained by the UCPC and CPC observations and investigated the consistency with the EEPS and SMPS measurements. We assumed log-normal number size distributions with various geometric mean diameters (GMDs) and geometric standard deviations (GSDs). We calculated the number fraction of sub-10 nm particles ($1 - \Delta N_{10}/\Delta N_{2.5}$) by integrating the number size distributions weighted by the penetration and detection efficiency curves:

Calculated sub-10 nm fraction = 1

$$-\left(\int \eta_{10\mathrm{CPC}}(\log D_p)\, n(\log D_p)\left(\frac{dN}{d\log D}\right) d\log D D_p\right)\Big/\left(\int \eta_{2.5\mathrm{UCPC}}(\log D_p)\, n(\log D_p)\left(\frac{dN}{d\log D}\right) d\log D D_p\right) \quad (4)$$

$$\text{Calculated EI}(N_{2.5}) = \int \eta_{\mathrm{UCPC}}\left(\frac{d\mathrm{EI}(N)}{d\log D}\right) d\log D \quad (5)$$

where $\eta_{10CPC}$ and $\eta_{2.5UCPC}$ are the overall penetration and detection efficiencies for the CPC $N_{10}$ and UCPC $N_{2.5}$, respectively~~, and $n$ is the assumed number size distribution function~~. We assumed monomodal size distributions for $dN/d\log D$ and $d\mathrm{EI}(N)/d\log D$ considering the shapes of the observed size distributions for the total and the non-volatile particles (Figs. 6 and 7). The overall penetration efficiency, which included the sampling tubes from the rooftop and the dilution/heater sections (~~see~~ Figs. 2 and ~~Fig. 4~~3b), was calculated based on the theoretical formulae by Gormley and Kennedy (1949). The GMD and GSD values assumed in Eq. (4) were also used to calculate the $d\mathrm{EI}(N)/d\log D$ in Eq. (5). The calculated $\mathrm{EI}(N_{2.5})$ was compared with the median $\mathrm{EI}(N_{2.5})$ derived from the observations to retrieve the absolute values of $d\mathrm{EI}(N)/d\log D$ and $\mathrm{EI}(N)$.

Fig. ~~10~~9 shows the calculation results~~.~~ ~~F~~for the total particles~~,~~. GMD values of <~~~~10 nm are needed to explain the median sub-10 nm fraction derived from the plume analysis (0.63) with a realistic range of GSDs (1.2–1.6). For example, the GMD value of 7.9 nm is obtained if we assume a GSD value of 1.6 (or the GMD value of 8.6 nm is obtained if we assume a GSD value of 1.4). The~~se results~~ retrieved $d\mathrm{EI}(N)/d\log D$ values ~~are~~were found to be consistent with ~~the measurements by~~those derived from the EEPS (Fig. ~~9~~8), which supports the validity of our estimate. The retrieved $\mathrm{EI}(N)$ value was $1.7 \times 10^{17}$ and $1.6 \times 10^{17}$ kg-fuel$^{-1}$ for (GMD, GSD) = (7.9 nm, 1.6) and (8.6 nm, 1.4), respectively. These values were larger by a factor of ~1.5 compared to the median total $\mathrm{EI}(N_{2.5})$ value, suggesting that the particle number EIs derived from the unheated UCPC might underestimate the true particle number EIs by a factor of ~1.5. ~~Fushimi et al. (2019) found the importance of jet engine lubrication oil as a source of aircraft exhaust particles with diameters ranging from ~10 to 30 nm. An important question arises from how lubrication oil contributes to the formation and growth of sub-10 nm particles. Future researches addressing this issue would be useful for developing a method for reducing particle emissions from aircraft.~~

Fig. 10 shows the calculation results ~~F~~for the non-volatile particles~~,~~. Similarly to the total particles, GMD values of <~~~~10 nm would also be needed to explain the median sub-10 nm fraction derived from the plume analysis (0.54)~~,~~. The GMD value of 9.0 nm is obtained if we assume a GSD value of 1.6 (or the GMD value of 9.5 nm is obtained if we assume a GSD value of 1.4). The retrieved $d\mathrm{EI}(N)/d\log D$ values were found to be consistent with those derived from the SMPS, although the size distribution data to support the validity of this estimate are limited. The retrieved $\mathrm{EI}(N)$ value was $1.0 \times 10^{16}$ and $0.95 \times 10^{16}$ kg-fuel$^{-1}$ for (GMD, GSD) = (9.0 nm, 1.6) and (9.5 nm, 1.4), respectively. These values were larger by a factor of ~1.7 compared to the median non-volatile $\mathrm{EI}(N_{2.5})$ value, suggesting that the particle number EI derived from the 350°C heated UCPC might underestimate the true non-volatile particle number EIs by a factor of ~1.7. ~~This feature is significantly different from the soot mode size distributions reported by previous studies (Petzold et al., 1999, Lobo et al., 2015a, Zhang et al., 2019).~~

### 4.2 Interpretation and implications

The characteristics of the total particles observed in this study are qualitatively consistent with the findings from previous studies (e.g., Petzold et al., 2005; Lobo et al., 2012, 2015b; Petzold et al., 1999; Kärcher et al., 2000; Brock et al., 2000): i.e., the total particle number EIs are dominated by volatile particles, and the sub-10 nm particles make significant

contributions to the total particle number EIs in the diluted plumes ($10^1$–$10^2$ m from the jet engines). In contrast to the total particles, the significance of sub-10 nm size ranges for the non-volatile particle number EIs is unexpected. Currently, we do not have direct evidence that the observed sub-10 nm non-volatile particles are composed mainly of soot. Nevertheless, it is worthwhile considering possible mechanisms for the formation of sub-10 nm non-volatile particles. Our estimate implies the presence of very small ~~soot~~non-volatile particles with diameters down to a few ~~nm~~nanometers. This is not consistent with the size of the primary soot particles from jet engines estimated by using transmission electron microscop~~y~~e (TEM) or laser-induced incandescence (LII) methods (e.g., Liati et al., 2014; Boies et al., 2015; Saffaripour et al., 2017, 2020), although there still remain substantial uncertainties in estimating the size of primary particles by those methods, as pointed out by Boies et al. (2015).

~~Currently we do not have direct evidences that the observed sub-10 nm non-volatile particles are composed mainly of soot. Nevertheless, it is worthwhile considering potential formation mechanisms of sub-10 nm soot particles. In general, the formation processes of soot particles from combustion sources are complicated and not fully understood (Johansson et al., 2018; Commodo et al., 2019). The whole mechanism, including inception and growth, takes place at high temperatures and on timescales of the order of a few milliseconds; moreover, sub-10 nm soot particles can be generated during the early stages of formation processes (Commodo et al., 2019). If combustion gases from jet engines immediately expand and are diluted on a timescale comparable to that for the formation of soot, significant numbers of sub-10 nm soot particles might be emitted to the atmosphere without the formation of larger agglomerates.~~

An alternative possibility for the significance of sub-10 nm non-volatile particles includes the potential contributions of less volatile organic matter~~s~~ (as compared with $C_{40}H_{82}$) or metal compounds. Fushimi et al. (2019) showed that the mass contribution of the sum of trace elements (other than carbonaceous and sul~~ph~~fur compounds) was comparable to that of elemental carbon (soot) for UFP samples (~10~~–~~–30 nm) collected at NRT. Saitoh et al. (2019a) ~~presented~~reported that metal elements including Ca, Fe, Si, Mg, K, Zn, Pb, and Ni were the major compositions of these trace elements. ~~Further investigations are needed to quantify the contributions of metal compounds to particle number concentrations.~~These metal compounds might have contributed to the non-volatile particles observed in this study.

The key point in our results is that the non-volatile particle number and volume EIs originating from soot-mode particles (>20 nm) were much smaller than those reported by the previous studies for take-off plumes under real-world operating conditions (Lobo et al., 2012, 2015b; Moore et al., 2017a). This feature might be related to the significance of sub-10 nm non-volatile particles. The data presented by Moore et al. (2017a), which were obtained in 2014, exhibited lower contributions of soot-mode particles compared to those by Lobo et al. (2012, 2015b), which were obtained in 2005 and 2004, respectively. A possible explanation for this tendency is that newer engines might emit smaller non-volatile particles as compared with older engines.

Our results have an implication for jet engine exhaust measurements by the SAE-ARP6320 method. The non-volatile $N_{10}$ data obtained from the 350°C heated CPC approximately correspond to the definition of non-volatile particles specified by SAE-ARP6320, at least in terms of the detectable size range of the particle counter and the removal efficiency of $C_{40}H_{82}$

particles (Section 3.1). If a population of non-volatile particles having a similar size distribution as shown in Fig. 10 is measured by the SAE-ARP6320 method, subtle changes in the size-dependent penetration and detection efficiencies of the measurement system and/or shifts in the mode diameter of the particle population might lead to large variabilities in the results. Further investigations are needed to quantify the size distributions of non-volatile particles for various types of engines under different conditions.

Our results also have an implication for the emission inventories of the aviation sector. Although the potential contributions of sub-10 nm particles inferred from our results likely have negligible impacts on the mass concentrations of ambient aerosol particles, they may have non-negligible impacts on the number concentrations in and around airports and also at aircraft cruising altitudes. The lifetime of sub-10 nm particles would be short near the ground level due to evaporative loss (e.g., Fushimi et al., 2008) and/or coagulation scavenging onto pre-existing larger particles, but it could be much longer under conditions of low temperatures and reduced concentrations of pre-existing aerosol particles. We propose that emissions of sub-10 nm particles from aircraft under real-world conditions should be properly considered for understanding the impacts of aviation on human health and also for developing aviation emission inventories for regional and global models.

## 5 Conclusions ~~and Implications~~

We conducted field measurements of aerosols at an observation point ~180 m from the centereline of a runway ~~of~~at Narita International Airport. We investigated the characteristics of particle emissions from in-use commercial aircraft under real-world operating conditions, with specific focuses on the contributions of sub-10 nm size ranges to total and non-volatile (350°C~~-~~ heated) particles. We used the UCPC, CPC, SMPS, and EEPS for the measurements of particle number concentrations and size distributions and carefully investigated the performance and consistency of these instruments. The major conclusions are summarized below.

- ~~The median total EI($N_{2.5}$) was ~60 times larger than the median non-volatile EI($N_{10}$) for the take-off plumes. This value can be interpreted as the difference between total particle number emissions under real-world conditions and non-volatile particle number emissions regulated by standard engine tests.~~ The median values of the total and the non-volatile EI($N_{2.5}$), which likely cover the major size range of aircraft emissions, were found to be 1.1 × $10^{17}$ and 5.7 × $10^{15}$ kg-fuel$^{-1}$, respectively. The difference in these values (a factor of ~20) is interpreted as the average contribution of volatile particles. We did not find a systematic dependence of the total particle number EIs on the estimated plume age (~30–120 s). The true particle number EIs for total and non-volatile particles might be larger by a factor of ~1.5 and ~1.7, respectively, compared to the above median values considering the penetration efficiencies through the sampling tubes and the evaporation tube.
- More than half ~~of~~the total and the non-volatile particle number EIs in the aircraft take-off plumes were found in the size range smaller than ~~~~10 nm ~~on average~~for most of the cases analyzed in this study. ~~The median sub-10 nm fraction in the~~

plumes was calculated to be 0.63 and 0.54 for total and non-volatile particles, respectively.The significance of sub-10 nm size ranges for the total particles was qualitatively consistent with previous studies, but that for the non-volatile particles was unexpected.

- The unheated UCPC, CPC, and EEPS data consistently suggest that the mode diameters of the $dEI(N)/d\log D$ for nucleation-mode particles obtained in this study were smaller than ~10 nm for the majority of the observed take-off plumes, and that the peak values of $dEI(N)/d\log D$ were larger than those previously reported under real-world operating conditions.
- The 350°C- heated UCPC, CPC, and SMPS and unheated EEPS data consistently suggest that the contributions of sub-10 nm size ranges to non volatile particle number EIs might be much higher than previously considered the non-volatile particle number and volume EIs originating from soot-mode particles (>20 nm) were much smaller than those reported by previous studies for take-off plumes under real-world operating conditions. Direct measurements of the chemical compositions of sub-10 nmnon-volatile particles are needed to investigate the mechanisms.

It should be noted that tThe characteristics of particle emissions may significantly depend on the type of jet engines, their maintenance conditions, and sulphur content of fuelsthe fuel sulfur content, which are not available in this study. Particle emissions may also depend on other factors including ambient pressure and temperature. These factors should be carefully considered for a more systematic comparison amongof different studies.

Although the potential contributions of sub-10 nm particles inferred from our results likely have small impacts on the mass concentrations of ambient aerosol particles, they may have non-negligible impacts on the number concentrations in and around airports and also at aircraft cruising altitudes. The lifetime of sub-10 nm particles would be short near the ground level due to evaporative loss (e.g., Fushimi et al., 2008) and/or coagulation scavenging onto pre-existing larger particles, but it could be much longer under conditions of low temperatures and reduced concentrations of pre-existing aerosol particles. We propose that emissions of sub-10 nm particles from aircraft under real-world conditions should be properly considered for understanding aviation impacts on human health and also for developing aviation emission inventories for regional and global models.

## Data availability

The field measurement data used in this study are provided as a supplementary material and will be available at a data repository.

## Author contributions

NT, AF, and HS designed the research; NT, AF, KM, YF, and KS performed field observations and collected data; NT, YM, and HS performed laboratory experiments; NT and YM performed data analysis; NT, AF, YF, and HS wrote the paper.

## Competing interests

The authors declare no conflict of interest.

## Acknowledgments

We thank Narita International Airport Corporation and Narita International Airport Promotion Foundation for their help during the field observations at Narita International Airport. We also thank Takumi Saotome at Research Institute for Environmental Strategies, Inc., Makiko Mine and Anna Nagasaki at Tokyo Metropolitan University for their help in the observations and data analysis, and Kenjiro Iida at AIST for useful advices on the evaluation of the UCPC and CPC. This study was funded by the Environment Research and Technology Development Fund (5-1709) of the Ministry of the Environment, Japan.

## References

Boies, A. M., Stettler, M. E. J., Swanson, J. J., Johnson, T. J., Olfert, J. S., Johnson, M., Eggersdorfer, M. L., Rindlisbacher, T., Wang, J., Thomson, K., Smallwood, G., Sevcenco, Y., Walters, D., Williams, P. I., Corbin, J., Mensah, A. A., Symonds, J., Dastanpour, R., and Rogak, S. N., Particle emission characteristics of a gas turbine with a double annular combustor, Aerosol Sci. Technol., 49, 842-855, doi:10.1080/02786826.2015.1078452, 2015.

Brock, C. A., Schröder, F., Kärcher, B., Petzold, A., Busen, R., and Fiebig, M.: Ultrafine particle size distributions measured in aircraft exhaust plumes, J. Geophys. Res., 105, 26555–26567, doi:10.1029/2000JD900360, 2000.

~~Commodo, M., Kaiser, K., De Falco, G., Minutolo, P., Schulz, F., D'Anna, A., and Gross, L.: On the early stages of soot formation: Molecular structure elucidation by high-resolution atomic force microscopy, Combust. Flame, 205, 154–164, 2019.~~

Durdina, L., Brem, B. T., Schönenberger, D., Siegerist, F., Anet, J. G., and Rindlisbacher, T.: Nonvolatile particulate matter emissions of a business jet measured at ground level and estimated for cruising altitudes, Environ. Sci. Technol., 53, 12865–12872, doi:10.1021/acs.est.9b02513, 2019.

Fushimi, A., Hasegawa, S., Takahashi, K., Fujitani, Y., Tanabe, K., and Kobayashi, S.: Atmospheric fate of nuclei-mode particles estimated from the number concentrations and chemical composition of particles measured at roadside and background sites, Atmos. Environ., 42, 949–959, doi:10.1016/j.atmosenv.2007.10.019, 2008.

Fushimi, A., Saitoh, K., Fujitani, Y., and Takegawa, N.: Identification of jet lubrication oil as a major component of aircraft exhaust nanoparticles, Atmos. Chem. Phys., 19, 6389–6399, doi:10.5194/acp-19-6389-2019, 2019.

Gormley, P. G., and Kennedy, M.: Diffusion from a stream flowing through a cylindrical tube, Proc. Royal Irish Acad. Sect. A, 52, 163–169, 1949.

Hagen, D. E., Whitefield, P. D., Paladino, J. D., and Trueblood, M. B.: Particulate sizing and emission indices for a jet engine exhaust sampled at cruise, Geophys. Res. Lett., 25, 1681–1684, doi:10.1029/97GL03504, 1998.

Herndon, S. C., Jayne, J. T., Lobo, P., Onasch, T. B., Fleming, G., Hagen, D. E., Whitefield, P. D., and Miake-Lye, R. C.: Commercial aircraft engine emissions characterization of in-use aircraft at Hartsfield-Jackson Atlanta International Airport, Environ. Sci. Technol., 42, 1877–1883, doi:10.1021/es072029+, 2008.

International Civil Aviation Organization, "Doc 10075. Assembly Resolutions in Force (as of 6 October 2016)" (ICAO, 2017; https://www.icao.int/Meetings/a39/Documents/Resolutions/10075_en.pdf).

~~Johansson, K. O., Head-Gordon, M. P., Schrader, P. E., Wilson, K. R., and Michelsen, H. A.: Resonance-stabilized hydrocarbon-radical chain reactions may explain soot inception and growth, Science, 361, 997–1000, 2018.~~

Jonsdottir, H. R., Delaval, M., Leni, Z., Keller, A., Brem, B. T., Siegerist, F., Schönenberger, D., Durdina, L., Elser, M., Burtscher, H., Liati, A., and Geiser, M.: Non-volatile particle emissions from aircraft turbine engines at ground-idle induce oxidative stress in bronchial cells, Commun. Biol., 2, 90, doi:10.1038/s42003-019-0332-7, 2019.

Kärcher, B., Turco, R. P., Yu, F., Danilin, M. Y., Weisenstein, D. K., Miake-Lye, R. C., Busen, R.: A unified model for ultrafine aircraft particle emissions, J. Geophys. Res., 105, 29379–29386, doi:10.1029/2000JD900531, 2000.

Kärcher, B., and Voigt, C.: Susceptibility of contrail ice crystal numbers to aircraft soot particle emissions, Geophys. Res. Lett., 44, 8037–8046, doi:10.1002/2017GL074949, 2017.

Kärcher, B.: Formation and radiative forcing of contrail cirrus, Nat. Commun., 9, 1824, doi:10.1038/s41467-018-04068-0, 2018.

Kinsey, J. S.: "Characterization of emissions from commercial aircraft engines during the Aircraft Particle Emissions eXperiment (APEX) 1 to 3" (EPA-600, R-09,130, EPA, 2009; https://cfpub.epa.gov/si/).

Kinsey, J. S., Squier, W., Timko, M., Dong, Y., and Logan, R.: Characterization of the fine particle emissions from the use of two Fischer–Tropsch fuels in a CFM56-2C1 commercial aircraft engine, Energy Fuels, 33, 8821–8834, doi:10.1021/acs.energyfuels.9b00780, 2019.

Lee, D. S., Pitari, G., Grewe, V., Gierens, K., Penner, J. E., Petzold, A., Prather, M. J., Schumann, U., Bais, A., Berntsen, T., Iachetti, D., Lim, L.L., and Sausen, R.: Transport impacts on atmosphere and climate: Aviation, Atmos. Environ., 44, 4678-4734, doi:10.1016/j.atmosenv.2009.06.005, 2010.

Liati, A., Brem, B. T., Durdina, L., Vögtli, M., Dasilva, Y. A. R., Eggenschwiler, P. D., and Wang, J., Electron microscopic study of soot particulate matter emissions from aircraft turbine engines, Environ. Sci. Technol., 48, 10975-10983, doi:10.1021/es501809b, 2014.

Lobo, P., Hagen, D. E., and Whitefield, P. D.: Measurement and analysis of aircraft engine PM emissions downwind of an active runway at the Oakland International Airport, Atmos. Environ., 61, 114-123, doi:10.1016/j.atmosenv.2012.07.028, 2012.

Lobo, P., Durdina, L., Smallwood, G. J., Rindlisbacher, T., Siegerist, F., Black, E. A., Yu, Z., Mensah, A. A., Hagen, D. E., Miake-Lye, R. C., Thomson, K. A., Brem, B. T., Corbin, J. C., Abegglen, M., Sierau, B., Whitefield, P. D., and Wang, J.:

Measurement of aircraft engine non-volatile PM emissions: Results of the Aviation-Particle Regulatory Instrumentation Demonstration Experiment (A-PRIDE) 4 campaign, Aerosol Sci. Technol., 49, 472–484, doi:10.1080/02786826.2015.1047012, 2015a.

Lobo, P., Hagen, D. E., Whitefield, P. D., and Raper, D.: PM emissions measurements of in-service commercial aircraft engines during the Delta-Atlanta Hartsfield Study, Atmos. Environ. 104, 237-245, doi: http://dx.doi.org/10.1016/j.atmosenv.2015.01.020, 2015b.

Masiol, M., and Harrison, R. M.: Aircraft engine exhaust emissions and other airport-related contributions to ambient air pollution: A review, Atmos. Environ., 95, 409–455, doi:10.1016/j.atmosenv.2014.05.070, 2014.

Moore, R. H., Shook, M. A., Ziemba, L. D., DiGangi, J. P., Winstead, E. L., Rauch, B., Jurkat, T., Thornhill, K. L., Crosbie, E. C., Robinson, C., Shingler, T. J., and Anderson, B. E.: Take-off engine particle emission indices for in-service aircraft at Los Angeles International Airport, Sci. Data, 4, 170198, doi:10.1038/sdata.2017.198, 2017a.

Moore, R. H., Thornhill, K. L., Weinzierl, B., Sauer, D., D'Ascoli, E., Kim, J., Lichtenstern, M., Scheibe, M., Beaton, B., Beyersdorf, A. J., Barrick, J., Bulzan, D., Corr, C. A., Crosbie, E., Jurkat, T., Martin, R., Riddick, D., Shook, M., Slover, G., Voigt, C., White, R., Winstead, E., Yasky, R., Ziemba, L. D., Brown, A., Schlager, H., and Anderson, B. E.: Biofuel blending reduces particle emissions from aircraft engines at cruise conditions, Nature, 543,411–415, doi:10.1038/nature21420, 2017b.

Oberdörster, G., Oberdörster, E., and Oberdörster, J.: Nanotoxicology: An emerging discipline evolving from studies of ultrafine particles, Environ. Health Perspect., 113, 823–839, doi:10.1289/ehp.7339, 2005.

Ohlwein, S., Kappeler, R., Joss, M. K., Künzli, N., and Hoffmann, B.: Health effects of ultrafine particles: a systematic literature review update of epidemiological evidence, Int. J. Public Health, 64, 547–559, doi:10.1007/s00038-019-01202-7, 2019.

Onasch, T. B., Jayne, J. T., Herndon, S., Worsnop, D. R., Miake-Lye, R. C., Mortimer, I. P., and Anderson, B. E.: Chemical properties of aircraft engine particulate exhaust emissions, J. Propul. Power, 25, 1121–1137, doi:10.2514/1.36371, 2009.

Petzold, A., Döpelheuer, A., Brock, C. A., and Schröder, F.: In situ observations and model calculations of black carbon emission by aircraft at cruise altitude, J. Geophys. Res., 104, D18, 22171–22181, doi:10.1029/1999JD900460, 1999.

Petzold, A., et al.: Particle emissions from aircraft engines - a survey of the European project PartEmis, Meteorologische Zeitschrift, 14, 465-476, doi:10.1127/0941-2948/2005/0054, 2005.

Righi, M., Hendricks, J., and Sausen, R.: The global impact of the transport sectors on atmospheric aerosol: simulations for year 2000 emissions, Atmos. Chem. Phys., 13, 9939-9970, doi:10.5194/acp-13-9939-2013, 2013.

Righi, M., Hendricks, J., and Sausen, R.: The global impact of the transport sectors on atmospheric aerosol in 2030 - Part 2: Aviation, Atmos. Chem. Phys., 16, 4481–4495, doi:10.5194/acp-16-4481-2016, 2016.

Saffaripour, M., Tay, L.-L., Thomson, K. A., Smallwood, G. J., Brem, B. T., Durdina L., and Johnson, M., Raman spectroscopy and TEM characterization of solid particulate matter emitted from soot generators and aircraft turbine engines, Aerosol Sci. Technol., 51, 518-531, doi:10.1080/02786826.2016.1274368, 2017.

Saffaripour, M., Thomson, K. A., Smallwood, G. J., and Lobo, P., A review on the morphological properties of non-volatile particulate matter emissions from aircraft turbine engines, J. Aerosol Sci., 139, 105467, doi:10.1016/j.jaerosci.2019.105467, 2020.

Saitoh K., Fushimi A., Fujitani F., Morino Y., Saotome T., Takegawa N. and Sera K.: Elemental composition of jet lubricating oil and fuel, and particles (particle size 10 nm-10 μm) collected near the Narita International Airport runway, Nishina Memorial Cyclotron Center Annual Report, 24 (fiscal year 2017), 41-52, published in 2019a (in Japanese).

Saitoh K., Fushimi A., Takegawa, N., and Sera, K.: Quantification of major and trace elements contained in aircraft JET A-1fuel by PIXE analysis, 35th PIXE Symposium, Tokyo, November 2019b (in Japanese).

Seinfeld, J. H., and Pandis, S. N.: Atmospheric Chemistry and Physics: From Air Pollution to Climate Change (Wiley, Hoboken, NJ, 2nd ed., 2006).

Society of Automotive Engineers, "Procedure for the continuous sampling and measurement of non-volatile particulate matter emissions from aircraft turbine engines: - Aerospace recommended practice 6320" (SAE International, 2018; https://saemobilus.sae.org/content/ARP6320/#scope).

Stacey, B.: Measurement of ultrafine particles at airports: A review, Atmos. Environ., 198, 463–477, doi:10.1016/j.atmosenv.2018.10.041, 2019.

Takegawa, N., and Sakurai, H.: Laboratory evaluation of a TSI condensation particle counter (Model 3771) under airborne measurement conditions, Aerosol Sci. Technol., 45, 272–283, doi:10.1080/02786826.2010.532839, 2011.

Takegawa, N., Moteki, N., Oshima, N., Koike, M., Kita, K., Shimizu, A., Sugimoto, N., and Kondo, Y.: Variability of aerosol particle number concentrations observed over the western Pacific in the spring of 2009, *J. Geophys. Res. Atmos.*, *119*, 13,474-13,488, doi:10.1002/2014JD022014, 2014.

Takegawa, N., Iida, K., and Sakurai, H.: Modification and laboratory evaluation of a TSI ultrafine condensation particle counter (Model 3776) for airborne measurements, Aerosol Sci. Technol., 51, 235–245, doi:10.1080/02786826.2016.1261990, 2017.

Takegawa, N., Seto, T., Moteki, N., Koike, M., Oshima, N., Adachi, K., Kita, K., Takami, A., and Kondo, Y.: Enhanced new particle formation above the marine boundary layer over the Yellow Sea: Potential impacts on cloud condensation nuclei, *J. Geophys. Res. Atmos.*, 125, e2019JD031448. https://doi.org/10.1029/2019JD031448, ~~in press~~2020.

Timko, M. T., Onasch, T. B., Northway, M. J., Jayne, J. T., Canagaratna, M. R., Herndon, S. C., Wood, E. C., Miake-Lye, R. C., and Knighton, W. B.: Gas turbine engine emissions: Part II: Chemical properties of particulate matter, J. Eng. Gas Turbines Power, 132, 061505, doi:10.1115/1.4000132, 2010.

Timko, M. T., Fortner, E., Franklin, J., Yu, Z., Wong, H. -W., Onasch, T. B., Miake-Lye, R. C., and Herndon, S. C.: Atmospheric measurements of the physical evolution of aircraft exhaust plumes, Environ. Sci. Technol., 47, 3513–3520, doi:10.1021/es304349c, 2013.

Wang, X. L., Grose, M. A., Avenido, A., Stolzenburg, M. R., Caldow, R., Osmondson, B. L., Chow, J. C., and Watson, J. G.: Improvement of engine exhaust particle sizer (EEPS) size distribution measurement - I. Algorithm and applications to compact aerosols, *J. Aerosol Sci.*, 92, 95–108, doi:10.1016/j.jaerosci.2015.11.002 , 2016.

Wang, Y., Liu, S .C., Anderson, B. E., Kondo, Y., Gregory, G. L., Sachse, G. W., Vay, S. A., Blake, D. R., Singh, H. B., and Thompson, A. M.: Evidence of convection as a major source of condensation nuclei in the northern midlatitude upper troposphere, Geophys. Res. Lett., 27, 369-372, doi:10.1029/1999GL010930, 2000.

Westerdahl, D., Fruin, S. A., Fine, P. L., and Sioutas, C.: The Los Angeles International Airport as a source of ultrafine particles and other pollutants to nearby communities, Atmos. Environ., 42, 3143–3155, doi:10.1016/j.atmosenv.2007.09.006, 2008.

Wiedensohler, A., Birmili, W., Nowak, A., Sonntag, A., Weinhold, K., Merkel, M., Wehner, B., Tuch, T., Pfeifer, S., Fiebig, M., Fjäraa, A. M., Asmi, E., Sellegri, K., Depuy, R., Venzac, H., Villani, P., Laj, P., Aalto, P., Ogren, J. A., Swietlicki, E., Williams, P., Roldin, P., Quincey, P., Hüglin, C., Fierz-Schmidhauser, R., Gysel, M., Weingartner, E., Riccobono, F., Santos, S., Grüning, C., Faloon, K., Beddows, D., Harrison, R., Monahan, C., Jennings, S. G., O'Dowd, C. D., Marinoni, A., Horn, H.-G., Keck, L., Jiang, J., Scheckman, J., McMurry, P. H., Deng, Z., Zhao, C. S., Moerman, M., Henzing, B., de Leeuw, G., Löschau, G., Bastian, S.: Mobility particle size spectrometers: Harmonization of technical standards and data structure to facilitate high quality long-term observations of atmospheric particle number size distributions, Atmos. Meas. Tech., 5, 657–685, doi:10.5194/amt-5-657-2012, 2012.

Wimmer, D., Lehtipalo, K., Franchin, A., Kangasluoma, J., Kreissl, F., Kürten, A., Kupc, A., Metzger, A., Mikkilä, J., Petäjä, T., Riccobono, F., Vanhanen, J., Kulmala, M., and Curtius, J.: Performance of diethylene glycol-based particle counters in the sub-3nm size range, Atmos. Meas. Tech., 6, 1793-1804, doi:10.5194/amt-6-1793-2013, 2013.

Yu, Z., Liscinsky, D. S., Fortner, E. C., Yacovitch, T. I., Croteau, P., Herndon, S. C., and Miake-Lye, R. C., Evaluation of PM emissions from two in-service gas turbine general aviation aircraft engines, Atmos. Environ., 160, 9-18, doi:10.1016/j.atmosenv.2017.04.007, 2017.

Yu, Z., Timko, M. T., Herndon, S. C., Miake-Lye, R. C., Beyersdorf, A. J., Ziemba, L. D., Winstead, E. L., and Anderson, B. E., Mode-specific, semi-volatile chemical composition of particulate matter emissions from a commercial gas turbine aircraft engine, Atmos. Environ., 218, 116974, doi:10.1016/j.atmosenv.2019.116974, 2019.

Zhang, X., Chen, X., and Wang, J.: A number-based inventory of size-resolved black carbon particle emissions by global civil aviation, Nat. Commun., 10, 534, doi:10.1038/s41467-019-08491-9, 2019.

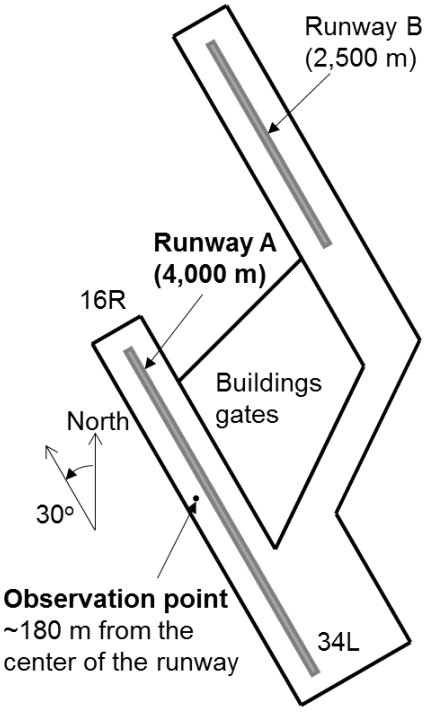


**Figure 1:** ~~An a~~Approximate layout of Narita International Airport (NRT). The observation point was located ~180 m from the centerline of runway A (~140 m from the edge of the runway). The azimuth of runway A is 30° from the north (23° from the magnetic north). The photograph shows the containers of instruments deployed at the observation point.

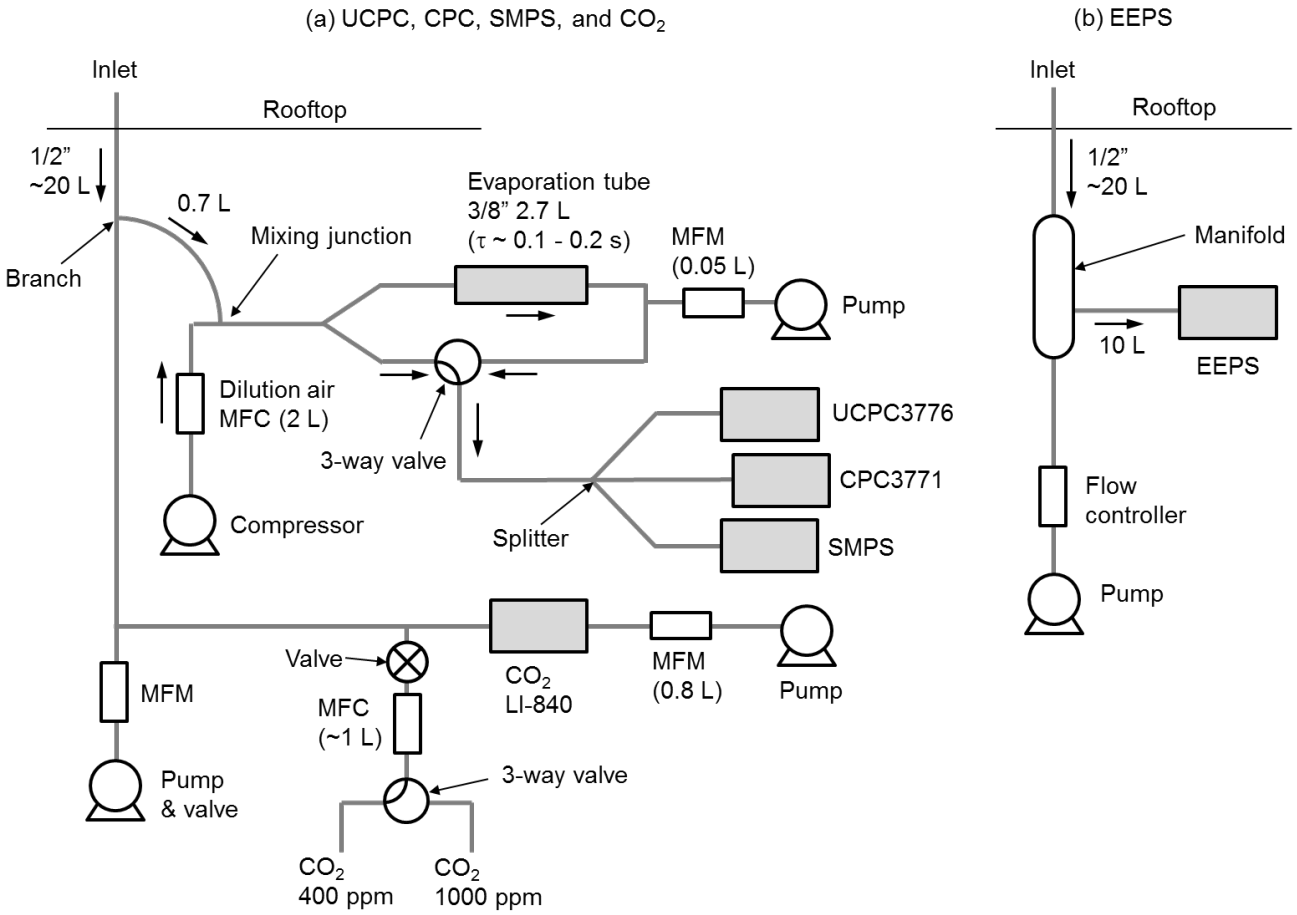


**Figure 2:** (a) Schematic of the sampling setup for the UCPC, CPC, SMPS, and $CO_2$ monitor. Ambient air was drawn into one of the two containers through a stainless steel tube and was split into a bypass flow ~~connecting to a piston pump~~ and sample flows for aerosols and $CO_2$. The aerosol sample flow was diluted by particle-free air regulated by a mass flow controller (MFC) to extend the concentration range measured by the UCPC and CPC. The diluted sample flow was then passed through a heated stainless-steel tube (evaporation tube) for heated sampling, or a bypass tube for unheated sampling. The flow was switched between the two paths by an automated three-way valve downstream. The tube downstream of the three-way valve was split into ~~the~~ individual sample flows for the UCPC, CPC, and SMPS. An additional small flow (~0.05 L min–1) was maintained by an orifice, a mass flow meter (MFM), and a pump to avoid the creation of a reverse stream from the evaporation tube during unheated sampling. (b) Schematic of the sampling setup for the EEPS. Ambient air was drawn into the other container through a copper tube, electrically conductive tubes, and a glass manifold. The sample flow for the EEPS was taken from the manifold. The total flow through the copper tube was maintained by a pump downstream of the manifold.

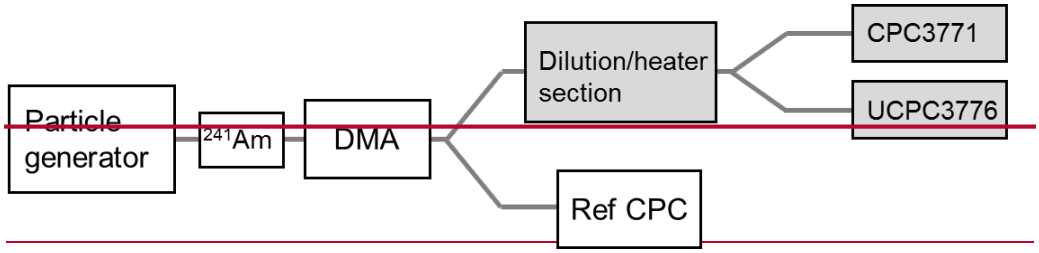


**Figure 3:** Experimental apparatus for the penetration and removal efficiencies experiments. An electrospray aerosol generator (EAG: Model 3480; TSI), a combustion aerosol standard (CAST; Matter Engineering) with a tube furnace for thermal treatment at 350°C, and a custom made tube furnace for supply of condensable vapours were used to generate polydisperse aerosol particles for the calibrations. Monodisperse aerosol particles were generated by using a bipolar charger conditioner (241Am) and a differential mobility analyzer (DMA). An aerosol electrometer (AE: Model 3068B; TSI) and a reference CPC (ref CPC: Model 3775; TSI) were used as reference instruments.

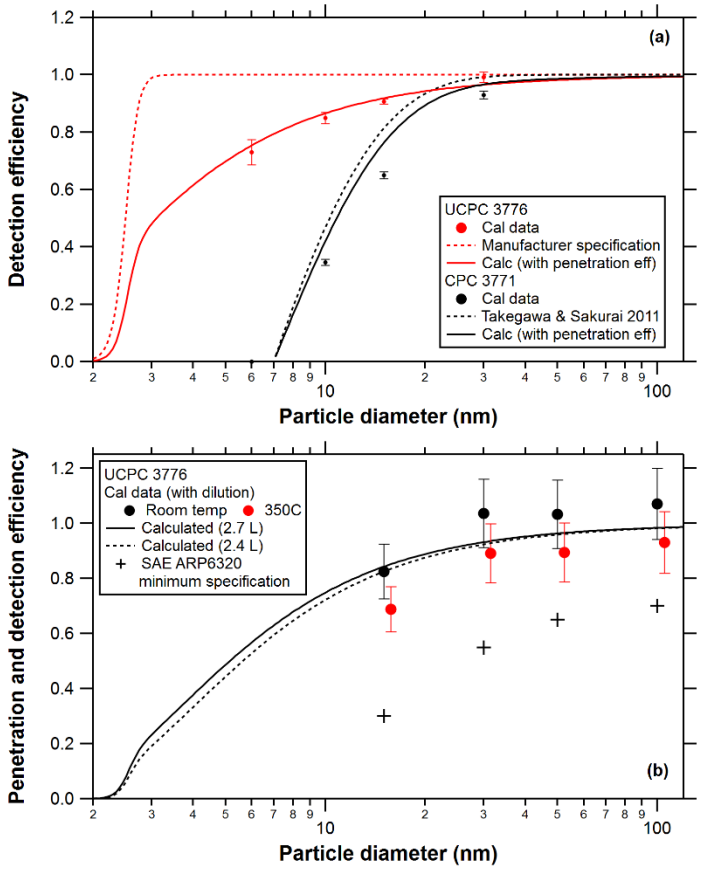


**Figure 43:** Laboratory evaluation of the performance of the UCPC and CPC. (a) Size-resolved detection efficiencies of the UCPC (red circles) and CPC (black circles) measured in the laboratory. The curves represent the empirically calculated detection and penetration efficiency curves for the UCPC and CPC: the detection efficiency of the UCPC (red dashed line); the detection efficiency of the UCPC incorporating the penetration efficiencies in the UCPC internal and sampling tube (red solid line); the detection efficiency of the CPC (black dashed line); and the detection efficiency of the CPC incorporating the penetration efficiency through the sampling tube (black solid line). See Section S1 of the Supplement for details on the definition. (b) Penetration and detection efficiency of non-volatile propane soot particles through the ~~heating mode sampling tubes~~heater section measured at room temperature (~19–21°C; black circles) and at 350°C (red circles). The calculated curves ~~includes~~ the penetration efficiency through the ~~dilution/~~heater section and the detection efficiency of the UCPC at 20°C~~room temperature~~ with the flow rate through the heater at 2.7 (solid) and 2.4 (dashed) L $min^{-1}$. The penetration efficiency curve at 350°C (not shown) was determined by scaling the calculated curve at 20°C with the experimental values at 350°C and room temperature for larger diameters (30, 50, and 100 nm). The cross symbols represent the minimum penetration efficiency of non-volatile particles specified by the SAE-ARP6320 protocol.

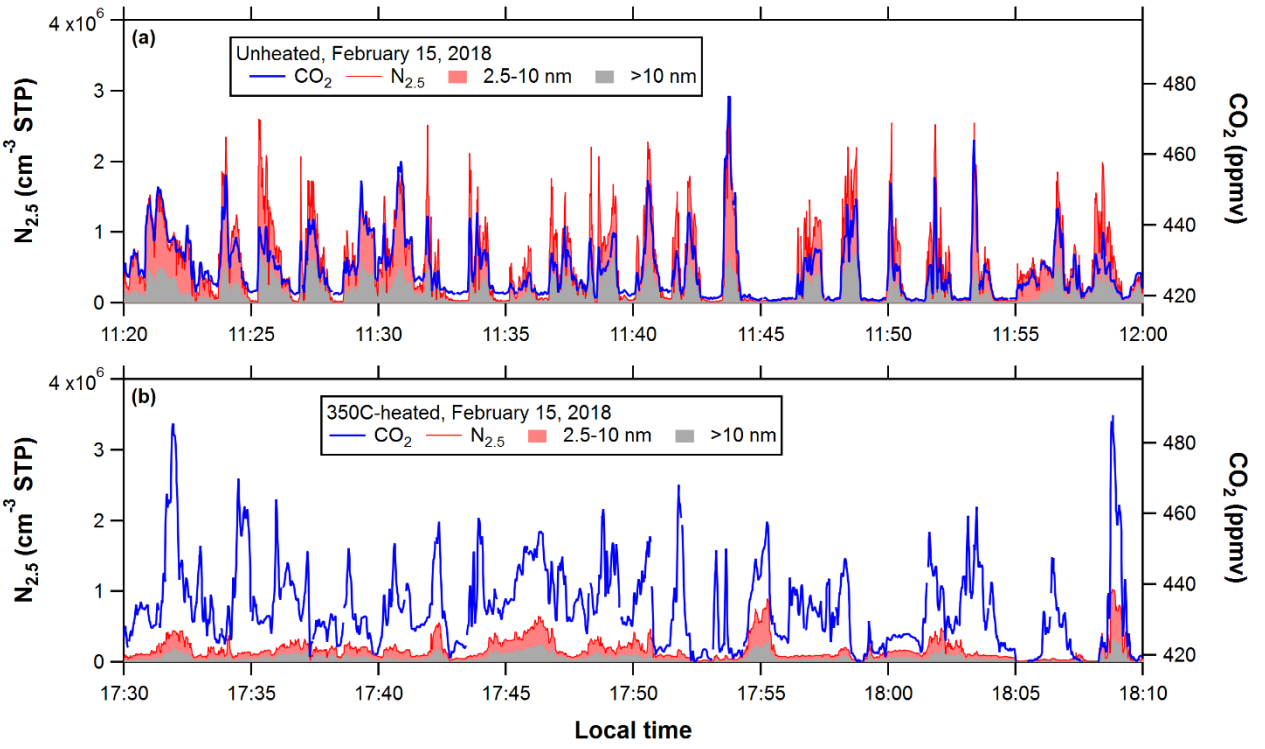


885

**Figure ~~54~~54:** Time series of $N_{2.5}$ and $CO_2$ observed near a runway ~~of~~at NRT. Data for (a) unheated and (b) 350°C~~-~~ heated modes obtained on February 15, 2018~~ are shown~~. The number fractions of particles with diameters ranging from 2.5 to 10 nm (red area) were generally larger than those for particles with diameters above 10 nm (gray area) for both the unheated and 350°C~~-~~ heated modes.

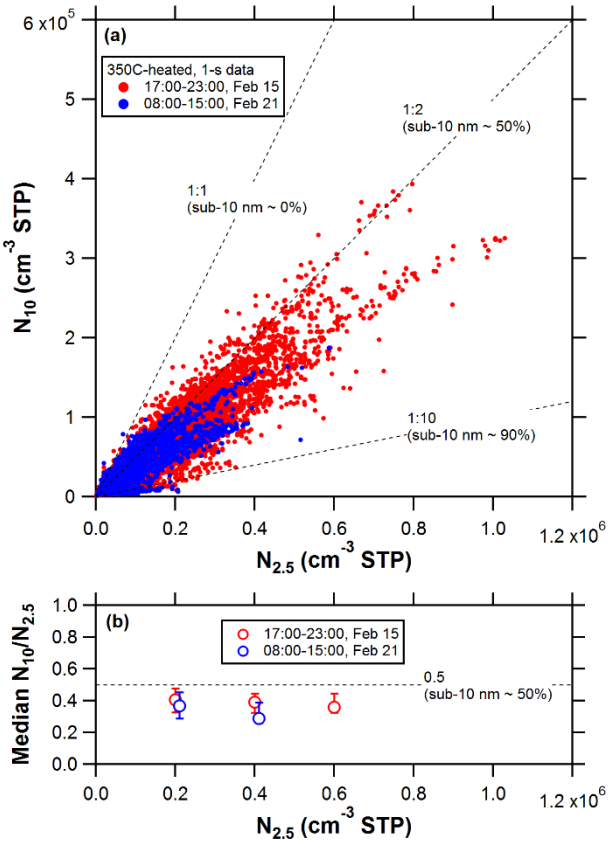


**Figure ~~6~~5:** (a) Scatterplots of $N_{10}$ versus $N_{2.5}$ for the 350°C- heated mode. Data obtained on February 15, 2018 (red) and February 21, 2018 (blue) are shown. The 1:1 correspondence line ($N_{10} = N_{2.5}$) represents the state in which all particles are included in the size range larger than 10 nm. (b) Median values of the $N_{10}/N_{2.5}$ ratios for the $N_{2.5}$ bin of (1–3) × $10^{15}$, (3–5) × $10^{15}$, and (5–7) × $10^{15}$ calculated by using the data shown in (a). The error bars represent the 25 and 75 percentile values.

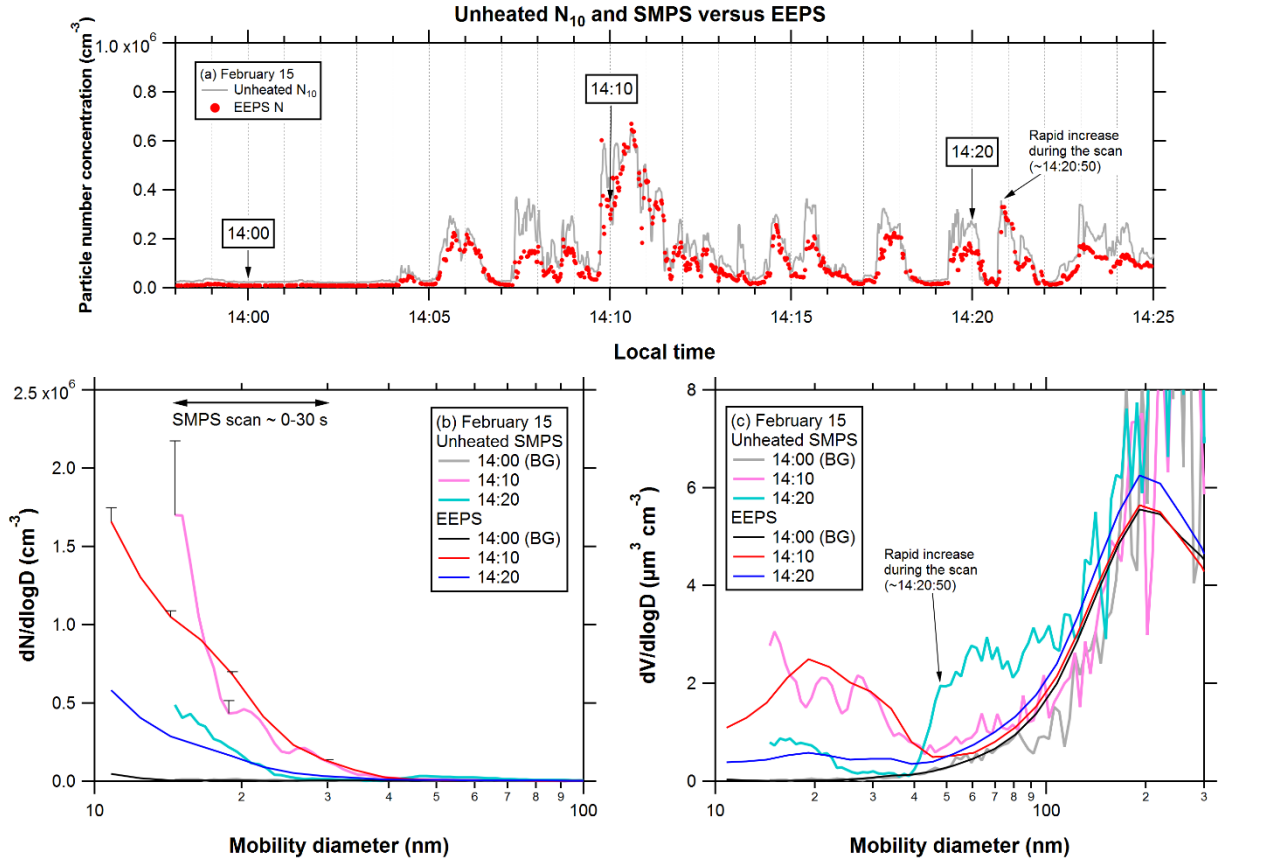


**Figure ~~7~~6:** (a) Time series of unheated $N_{10}$ (gra~~e~~y) and total particle number concentrations derived from the EEPS data (EEPS N, red) obtained at 13:58–~~–~~14:25 LT on February 15, 2018. (b) Particle number size distributions ~~as~~ measured simultaneously by the EEPS and unheated SMPS for selected time periods indicated in (a). The EEPS data were averaged over 40 s around the timing of the SMPS scan corresponding to the diameter range of 15–30 nm (i.e., averaged from 10 s before to 30 s after the onset of each SMPS scan). "BG" denotes a time period without enhancements of the aerosols and $CO_2$. The upper ends of the error bars indicate the particle number concentrations incorporating the penetration efficiencies of particles through the sampling tubes shown in Fig. S1. (c) Same as (b) but for the particle volume size distributions.

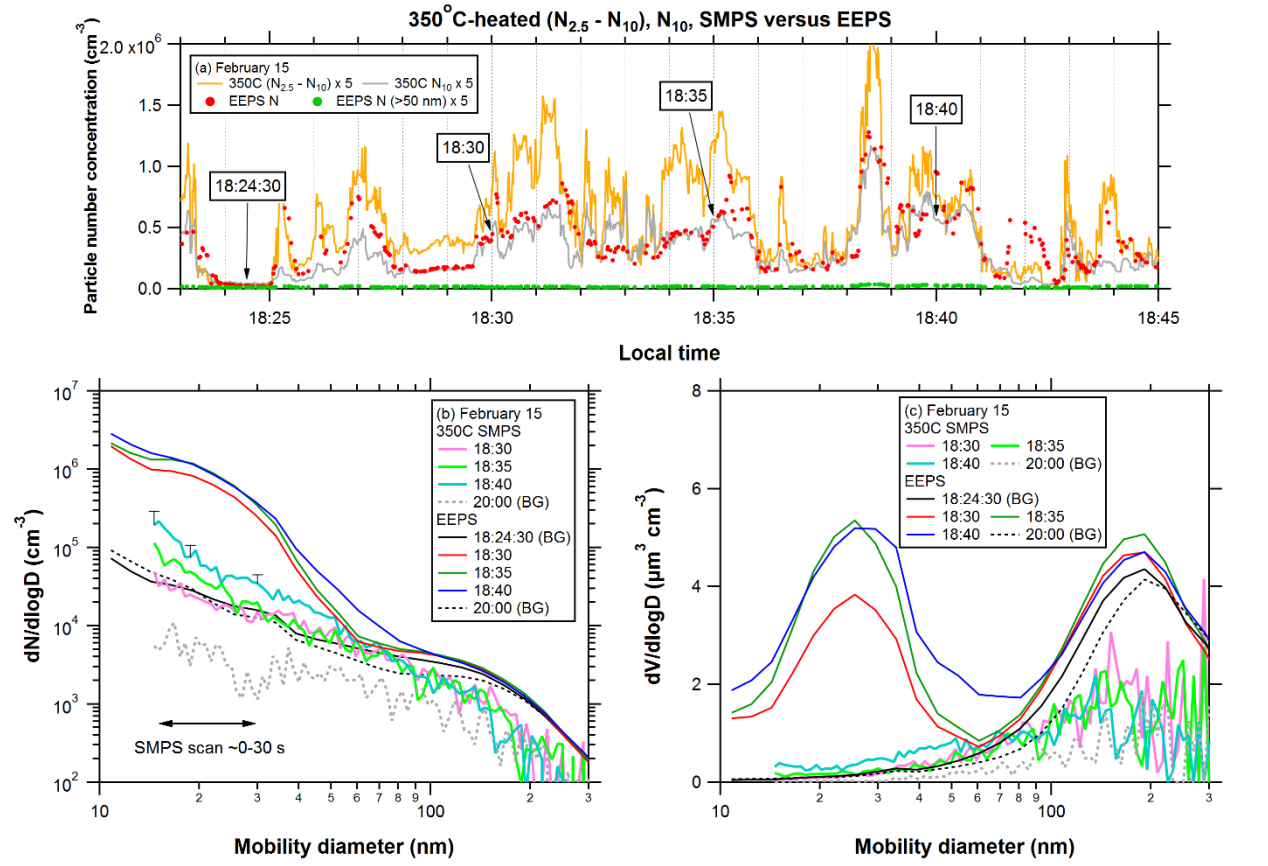


**Figure ~~8~~7:** (a) Time series of 350°C~~-~~ heated $N_{2.5} - N_{10}$ (orange), $N_{10}$ (gra~~e~~y), total particle number concentrations derived from the EEPS data (EEPS N, red), and particle number concentrations for a diameter range of >50 nm measured by the EEPS (EEPS N (>50 nm), ~~orange~~green) obtained at 18:23~~–~~18:45 LT on February 15, 2018. The 350°C~~-~~ heated $N_{2.5} - N_{10}$, $N_{10}$, and EEPS N (>50 nm) data are multiplied by a factor of 5 for clarity. (b) Particle number size distributions ~~as~~ measured simultaneously by the EEPS and 350°C~~-~~ heated SMPS for selected time periods indicated in (a). The average method for the EEPS is the same as that used in Fig. ~~7~~6b. "BG" denotes a time period without enhancements of the aerosols and $CO_2$. The upper ends of the error bars indicate the particle number concentrations incorporating the penetration efficiencies of particles through the sampling tubes and evaporation tube (Figs. 3 and S1). (c) Same as (b) but for the particle volume size distributions.

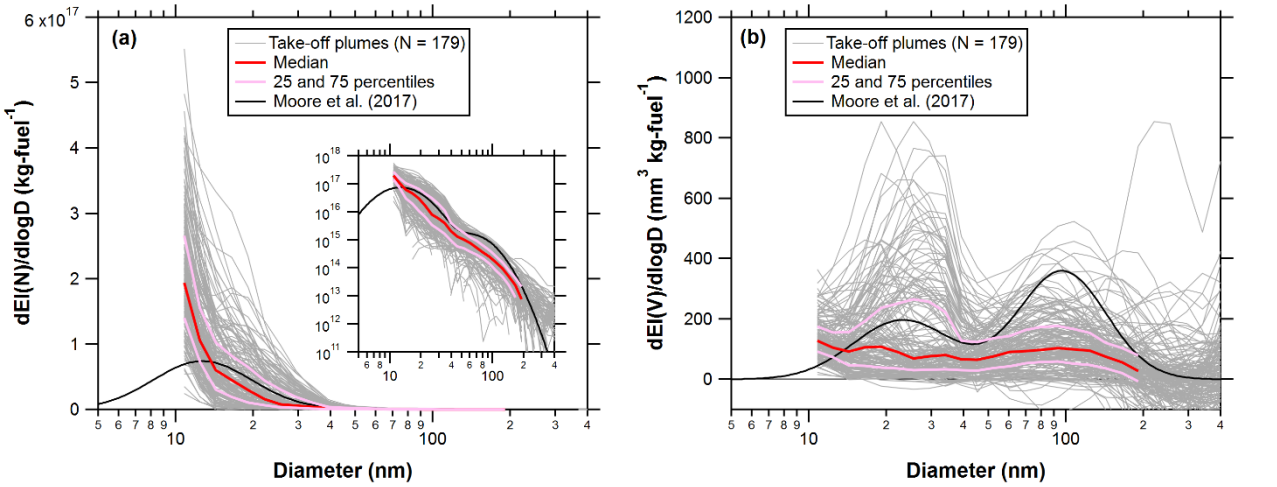


925

**Figure ~~9~~8:** Size distributions of (a) number and (b) volume EIs derived from the EEPS data for the take-off plumes. The penetration efficiencies of particles through the sampling tubes (Fig. S1) are incorporated in these estimates. The shaded lines represent all data for the take-off plumes. The red and two pink lines indicate the median, 25, and 75 percentiles, respectively. The black line represents the average size distributions from Moore et al. (2017a). A log-log plot of the same data is inserted in (a) for better visualization of the smaller values.

930

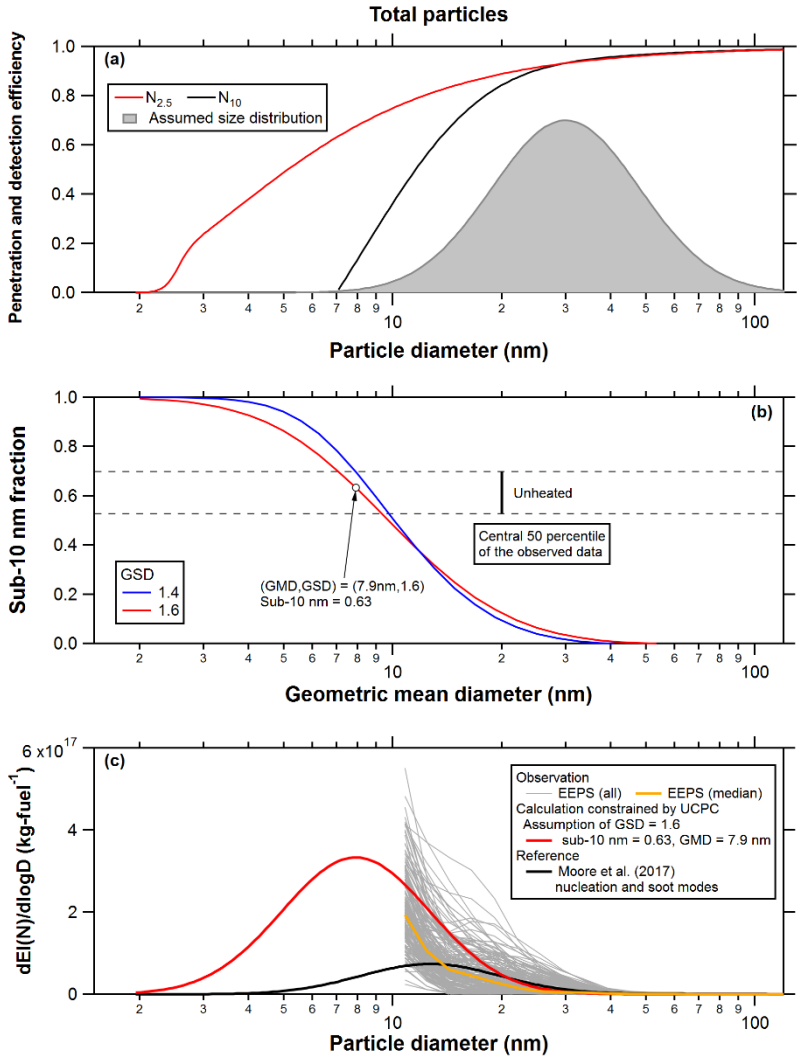


**Figure ~~10~~9:** (a) Overall penetration and detection efficiencies for the unheated ~~and 350°C-heated~~ $N_{2.5}$ and $N_{10}$. ~~The lower limit of the penetration efficiency through the VPR specified in SAE ARP6320 is shown for comparison.~~ The shaded area represents an example of the assumed particle number size distributions for calculating the number fraction of sub-10 nm particles. (b) Number fraction of sub-10 nm particles ($1 - \Delta N_{10}/\Delta N_{2.5}$) obtained by convolution of the penetration and detection efficiency curves in (a) and assumed particle number size distributions having various GMDs and GSDs. The horizontal dashed lines indicate the central 50 percentile range (between 25 and 75 percentiles) of the observed data for the unheated ~~and 350°C-heated~~ mode. ~~The calculation results for the unheated and 350°C-heated modes were nearly identical because we assumed that the size-dependency of the penetration efficiency of particles through the evaporation tube for the 350°C-heated mode was the same as that for the unheated mode.~~ (c) ~~An e~~Example of the particle number EI size distributions that ~~can~~ explains the observed medians of the $\Delta N_{10}/\Delta N_{2.5}$ ratios and EI($N_{2.5}$) for the unheated mode (red). The number EI size distributions with (GMD, GSD) = (12.7 nm, 1.56) and (61 nm, 1.48), which correspond to the average "nucleation ~~mode~~" and "soot mode" distributions (~~blue and~~ black~~, respectively~~) reported by Moore et al. (2017a), are shown for comparison. The size distributions of particle number EIs for the take-off plumes derived from the EEPS data (Fig. ~~9~~8a) ~~and particle number size distributions obtained by the 350°C-heated SMPS on February 15, 2018 (Fig. 8b)~~ are also shown.

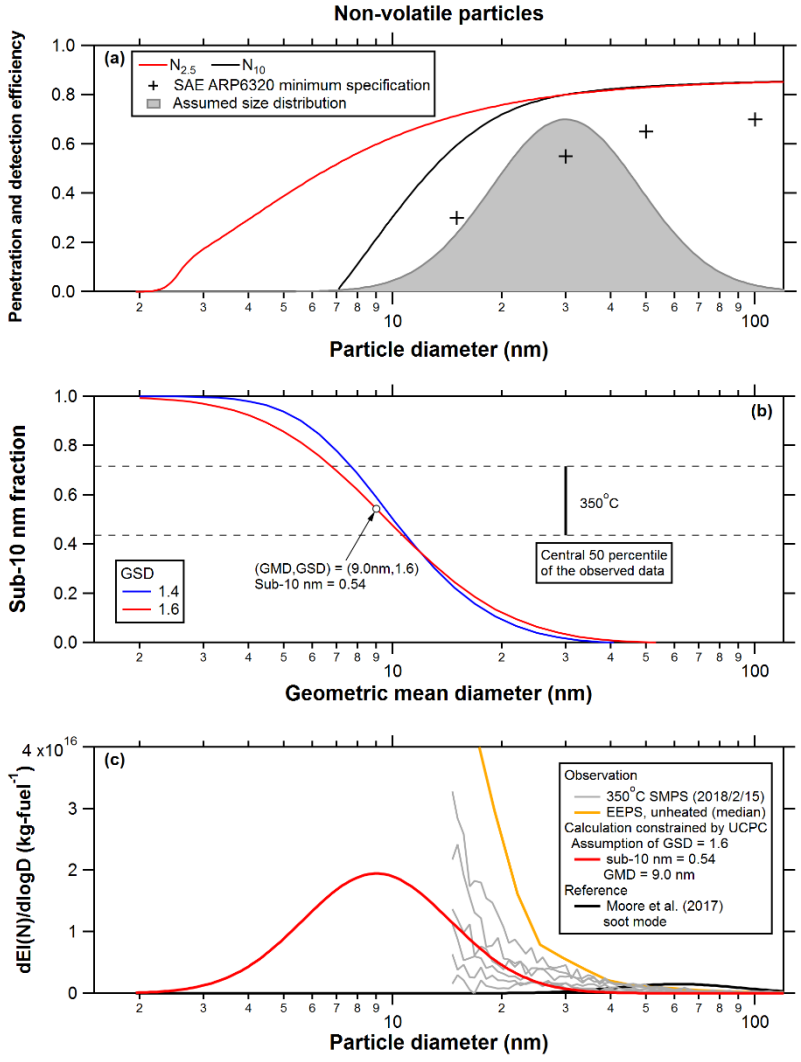


**Figure 10:** (a) Overall penetration and detection efficiencies for the 350°C heated $N_{2.5}$ and $N_{10}$. The lower limit of the penetration efficiency through the VPR specified in SAE-ARP6320 is shown for comparison. The shaded area represents an example of the assumed particle number size distributions for calculating the number fraction of sub-10 nm particles. (b) Number fraction of sub-10 nm particles ($1 - \Delta N_{10}/\Delta N_{2.5}$) obtained by convolution of the penetration and detection efficiency curves in (a) and assumed particle number size distributions having various GMDs and GSDs. The horizontal dashed lines indicate the central 50 percentile range (between 25 and 75 percentiles) of the observed data for the 350°C heated mode. The calculation results for the unheated (Fig. 9b) and 350°C heated modes were nearly identical because we assumed that the size dependency of the penetration efficiency of particles through the evaporation tube for the 350°C heated mode was the same as that for the unheated mode. (c) Examples of the particle number size distributions that can explain the observed median of $\Delta N_{10}/\Delta N_{2.5}$ ratios for the 350°C heated mode (red). The size distribution of particle number EI with (GMD, GSD) = (61 nm, 1.48), which corresponds to the average soot mode distribution (black) reported by Moore et al. (2017a), is shown for comparison. The size distributions of particle number EIs for the take-off plumes estimated from the 350°C heated SMPS on February 15, 2018 are also shown. The penetration efficiencies of particles through the sampling tubes and evaporation tube (Figs. 3 and S1) are incorporated in the SMPS estimates.

**Table 1:** Remaining fraction (%) of tetracontane ($C_{40}H_{82}$) particles measured by the UCPC and CPC downstream of the evaporation tube.

| Particle size | 30 nm | 43 nm | 50 nm |
|---|---|---|---|
| UCPC | 0.3 (+0.2/–0.0) | 1.9 (+1.4/–0.2) | 5.4 (+4.1/–0.5) |
| CPC | <0.1 | <0.1 | <0.1 |

965

**Table ~~1~~2:** Particle number emission indices (EIs) (particles kg-fuel~~s~~$^{-1}$) and sub-10 nm fractions. ~~The particle number EI values for unheated $N_{2.5}$, unheated $N_{10}$, 350°C-heated $N_{2.5}$, and 350°C-heated $N_{10}$ are referred to as total EI($N_{2.5}$), total EI($N_{10}$), non-volatile EI($N_{2.5}$), and non-volatile EI($N_{10}$), respectively.~~

| | 25 percentile | 50 percentile | 75 percentile |
|---|---|---|---|
| Total | | | |
| EI($N_{2.5}$) | $8.9 \times 10^{16}$ | $1.1 \times 10^{17}$ | $1.3 \times 10^{17}$ |
| EI($N_{10}$) | $3.2 \times 10^{16}$ | $4.2 \times 10^{16}$ | $5.2 \times 10^{16}$ |
| Sub-10 nm fraction | 0.53 | 0.63 | 0.70 |
| Non-volatile | | | |
| EI($N_{2.5}$) | $2.4 \times 10^{15}$ | $5.7 \times 10^{15}$ | $1.1 \times 10^{16}$ |
| EI($N_{10}$) | $1.1 \times 10^{15}$ | $1.8 \times 10^{15}$ | $4.0 \times 10^{15}$ |
| Sub-10 nm fraction | 0.44 | 0.54 | 0.72 |

Note: The particle number EI values for unheated $N_{2.5}$, unheated $N_{10}$, 350°C-heated $N_{2.5}$, and 350°C heated $N_{10}$ are referred to as total EI($N_{2.5}$), total EI($N_{10}$), non-volatile EI($N_{2.5}$), and non-volatile EI($N_{10}$), respectively.

970

*Supplement of*

# Characteristics of sub-10 nm particle emissions from in-use commercial aircraft observed at Narita International Airport

Nobuyuki Takegawa, et al.

*Correspondence to*: Nobuyuki Takegawa (takegawa@tmu.ac.jp)

## S1 Penetration efficiencies of particles through the sampling tubes

The penetration efficiencies of particles through the sampling tubes were estimated by using the theoretical formulae proposed by Gormley and Kennedy (1949). The calculations assumed a laminar flow at a pressure of 101 kPa and a temperature of 293 K. The inlet system was divided into the subsections listed in Table S1, and the overall penetration efficiency was derived as a product of the penetration efficiencies through the subsections. The subsection "UCPC internal" in Table S1 represents the effective tube length that can reproduce the penetration efficiency through a UCPC 3776 (Wimmer et al., 2013). The detection efficiencies of the UCPC and CPC, which are denoted as $\varepsilon_{UCPC}$ and $\varepsilon_{CPC}$, were set as follows based on our previous studies (Takegawa and Sakurai, 2011; Takegawa et al., 2017):

$$\varepsilon_{UCPC} = \left(1 + \exp\left(\frac{2.50 - D}{0.111}\right)\right)^{-1}$$

$$\varepsilon_{CPC} = 1 - \exp\left(\frac{6.99 - D}{4.78}\right)$$

where $D$ is the particle diameter. Note that the detection efficiency for the UCPC was empirically determined so as to satisfy $\varepsilon_{UCPC}$ = ~0, 0.5, ~1 at diameters of <2, 2.5, >3 nm, respectively. This assumption does not significantly affect the major conclusions because the contributions of particles at 2–3 nm were minor in the theoretical calculations (Figs. 9 and 10). As shown in Fig. 3, the detection efficiencies of the UCPC and CPC incorporating the penetration efficiencies of the subsections agreed well with the experimental data.

Fig. S1 shows the penetration efficiency for the UCPC/CPC sampling line under the unheated mode (UCPC/CPC main × UCPC/CPC total sample × Unheated), that for the SMPS sampling line under the unheated mode (UCPC/CPC main × UCPC/CPC total sample × Unheated × SMSP sample), and that for the EEPS sampling line (EEPS main × EEPS sample). The penetration efficiency through the evaporation tube and the detection efficiencies of the UCPC and CPC were evaluated separately from the above estimates (see Section 3.1).

**Table S1:** Parameters for calculating the penetration efficiencies of particles for the UCPC, CPC, SMPS, and EEPS.

| Subsection | Flow rate (L $min^{-1}$) | Length (cm) | Penetration efficiency at 10 nm |
|---|---|---|---|
| UCPC/CPC main (rooftop – branch) | 20 | 280 | 0.97 |
| UCPC/CPC total sample (branch – mixing junction) | 0.7 | 30 | 0.94 |
| Unheated (mixing junction – splitter) | 2.7 | 67 | 0.96 |
| Heated (mixing junction – heater – splitter) | 2.7 | 152 | 0.92 |
| UCPC sample (splitter – UCPC) | 1.4 | 50 | 0.94 |
| CPC sample (splitter – CPC) | 1.0 | 90 | 0.90 |
| SMPS sample (splitter – SMPS) | 0.3 | 100 | 0.77 |
| UCPC internal | 0.3 | 19 | 0.92 |
| EEPS main (rooftop – manifold branch) | 20 | 276 | 0.97 |
| EEPS sample (manifold branch – EEPS) | 10 | 100 | 0.97 |

Note: See Fig. 2 for the schematics of the subsections. The flow rate and length of each section are approximate values.

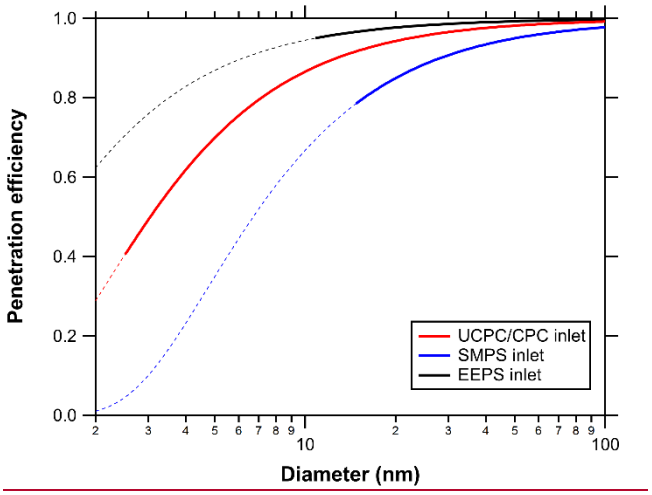


**Figure S1:** Penetration efficiencies of particles through the sampling lines for the UCPC/CPC (red), SMPS (blue), and EEPS (black) at room temperature (293 K) estimated by using the theoretical formulae proposed by Gormley and Kennedy (1949). The detectable size ranges for the UCPC, SMPS, and EEPS are indicated by solid lines. The calculated curve for the UCPC/CPC includes the penetration efficiency through the UCPC/CPC main, UCPC/CPC total sample, and Unheated subsections. The calculated curve for the SMPS includes the penetration efficiencies through the UCPC/CPC main, UCPC/CPC total sample, Unheated, and SMSP sample subsections. The calculated curve for the EEPS includes the penetration efficiencies through the EEPS main and EEPS sample subsections.

## S2 Diffusion correction for the SMPS

The Aerosol Instrument Manager (AIM) software provides correction tools for these factors. We used AIM version 9.0 for the present analysis, with the diffusion loss correction enabled. Fig. S2 shows a comparison of the SMPS size distribution at 14:10 on February 15, 2018 with and without the AIM diffusion correction. The degree of correction was significant at smaller diameters. Nevertheless, the overall size dependency (i.e., increasing particle number concentrations with decreasing particle diameters below 20 nm) is consistent between the SMPS and EEPS data, regardless of the AIM diffusion correction.

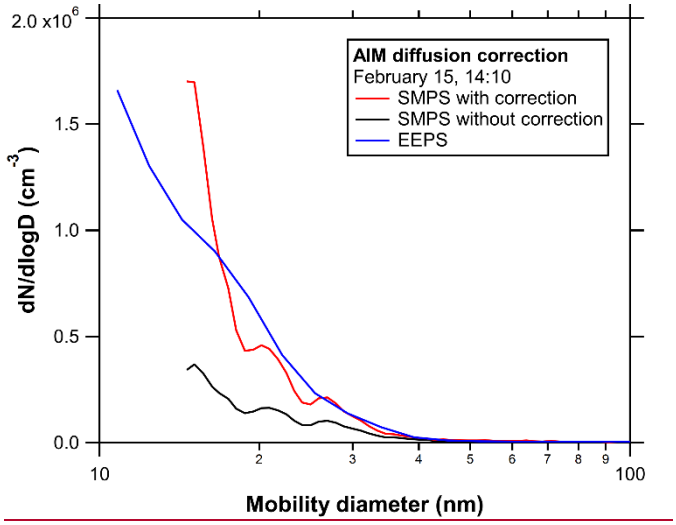


**Figure S2:** Particle number size distributions measured simultaneously by the EEPS and unheated SMPS (with and without the AIM diffusion correction) for the selected time period indicated in Fig. 6.

**S~~1~~3 Plume analysis**

In the observed air parcels, aircraft emissions from take-off, landing, and idling phases may have been mixed in the atmosphere, and the characterization of particle emissions should be performed carefully. The distance from the observation point to the taxiway was ~380 m and that to the gate was >800 m. We expected that aircraft emissions during idling would contribute to relatively broad, diffuse increases in aerosols and $CO_2$ and that those during take-off and landing would appear as spiked increases in aerosols and $CO_2$ at the observation point.

To extract discrete plumes originating from individual aircraft during take-off or landing, we defined background levels for $N_{2.5}$, $N_{10}$, and $CO_2$, and calculated enhancements above the background levels ($\Delta N_{2.5}$, $\Delta N_{10}$, and $\Delta CO_2$). The background estimate is more critical for $CO_2$. For air parcels originating from the runway (wind directions from north to east-southeast, wind speeds of >1 m $s^{-1}$), the sets of air parcels that were selected by the following procedures were defined as "plumes":

(a) The background air was defined as satisfying the following conditions: $|\, dCO_2/dt \,| < 0.1$ ppmv $s^{-1}$, $|\, d^2CO_2/dt^2 \,| < 0.1$ ppmv $s^{-2}$, $|\, dN_{10}/dt \,| < 500$ $cm^{-3}$ $s^{-1}$, and $N_x < N_{th}$, ($x$ = 2.5 or 10) where $d/dt$ represents the time differential. The second and fourth conditions were set to exclude plume peaks. The threshold value, $N_{th}$, depended~~s~~ on the meteorological conditions and was set to an appropriate values for each day.

(b) The above background values were interpolated to determine the baselines for $N_{2.5}$, $N_{10}$, and $CO_2$. The baseline was subtracted to obtain $\Delta N_{2.5}$, $\Delta N_{10}$, and $\Delta CO_2$.

(c) If the peak $\Delta CO_2$ exceeded 15 ppmv, the $\Delta CO_2$ values decreased to below 10% of the peak value within 60 s before or after the peak, and the duration of the enhancement was longer than 30 s, the set of air parcels was selected as a "plume".

The above threshold values were determined by considering the observed shapes of the $CO_2$ and aerosol spikes. Step (a) was used to identify "stable" baseline data points, and the conditions were set as redundant. The criterion of 10% in step (c) eliminated overlaps of multiple plumes. This automated procedure may have discarded some possible plume events, depending on the meteorological condition. Nevertheless, we chose these criteria to avoid subjective biases.

Next, the $\Delta N_{2.5}/\Delta CO_2$, $\Delta N_{10}/\Delta CO_2$, and $\Delta N_{10}/\Delta N_{2.5}$ ratios for the identified plumes were calculated. Only data with $N_{10}$ smaller than $5 \times 10^5$ $cm^{-3}$ (~$1 \times 10^5$ $cm^{-3}$ downstream of the dilution section) were used for the analysis because the uncertainty due to particle coincidence increases at higher concentrations. Data obtained on February 15, 16, 20, 21, and 22 were used for the plume analysis. The $\Delta N_{2.5}/\Delta CO_2$, $\Delta N_{10}/\Delta CO_2$, and $\Delta N_{10}/\Delta N_{2.5}$ ratios were calculated by using an area-integration method, similar to that used by Moore et al. (2017a). We also calculated these ratios as linear regression slopes after the data points were averaged over 3 s. The data average was used to account for differences in the response times of the instruments. Although these two methods generally showed reasonable agreement, there were significant discrepancies in some cases, especially at low $r^2$ values by the regression method. The reason for the discrepancy at low $r^2$ values was ~~because~~that the temporal variations in $N_{2.5}$ and $N_{10}$ did not track well with that of $CO_2$. A possible explanation for this feature

is that particle emissions might vary significantly during take-off (e.g., a burst of soot particles in the initial stages), as pointed out by Moore et al. (2017a).

The arrival time of a plume was estimated by considering the wind directions and speeds, assuming that the time for the plume to traverse from the centerline of the runway to the observation point was controlled by the wind vector component perpendicular to the runway. The duration of a plume was estimated from the time difference between the two 10%-crossing points defined in step (c) (when the $\Delta CO_2$ values decreased to below 10% of the peak value within 60 s before or after the peak). The estimated arrival time of plumes was ~30–120 s, which corresponds to the transport distance of ~180–370 m.

The flight-schedule table provided by NRT, which specified the take-off or landing times of specific aircraft with a time resolution of 1 min, was used to investigate the statistics of aircraft take-offs and landings. During the time periods of the plume analyses, 80–90% of the aircraft that passed along the runway were in the take-off phases. The flight-schedule table, estimated arrival times, and our video-camera records (only during the daytime) were used to attribute the observed plumes to take-off or landing phases. Fig. S13 shows an example of the correspondence between the plume events and the flight information. Aerosol particle number concentrations for diameters larger than 7 nm ($N_7$) as measured by the undiluted and unheated CPC 3022 are shown for comparison. In Fig. S13a, we can see a reasonably good agreement between $N_7$ and $N_{10}$, as expected. In Fig. S13b, the depletion of aerosol particle number concentrations upon heating is evident.

Although the observed plumes could, in most cases, be attributed to the take-off or landing of specific aircraft, there were some cases in which the one-to-one correspondence was somewhat ambiguous (shown as "unidentified" in Fig S13a). We attributed 132 plumes to take-offs for the unheated mode and 63 plumes to the 350°C-heated mode. Potential uncertainties in the attribution (i.e., a landing plume incorrectly assigned to a take-off plume) are 10–20% at most, considering that 80–90% of the aircraft that passed along the runway were in the take-off phases. Table S12 shows the statistical summary of the particle number EIs classified by major aircraft models identified in this study. We did not observe a significant difference in the particle number EIs among these models, although there might be uncertainties in the attribution, as mentioned above.

Fig. S24 shows histograms of the estimated arrival time and duration of the plumes. Although our sampling conditions differed from those given by Moore et al. (2017a), the estimated arrival and duration times were comparable to their values. We did not find a systematic dependence of the $\Delta N_{10}/\Delta CO_2$ and $\Delta N_{2.5}/\Delta CO_2$ ratios on the arrival time of the plumes, as indicated in Fig. S35.

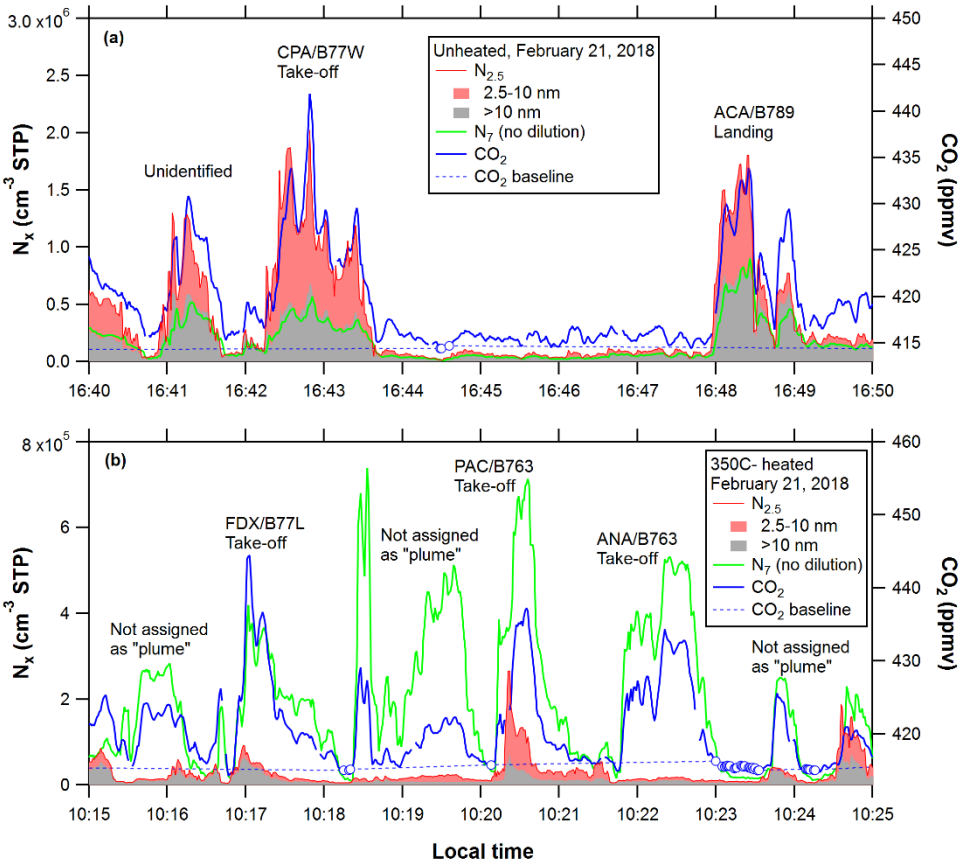


120 **Figure S~~1~~3:** Examples of discrete plumes. Data for (a) unheated and (b) 350°C- heated mode observed on February 21, 2018 ~~are shown~~. Slight differences in the peak timing for very sharp spikes may be affected by the instrument response times. The blue open circles represent the estimated "background" concentrations for $CO_2$, and the blue dashed lines represent the interpolated background levels.

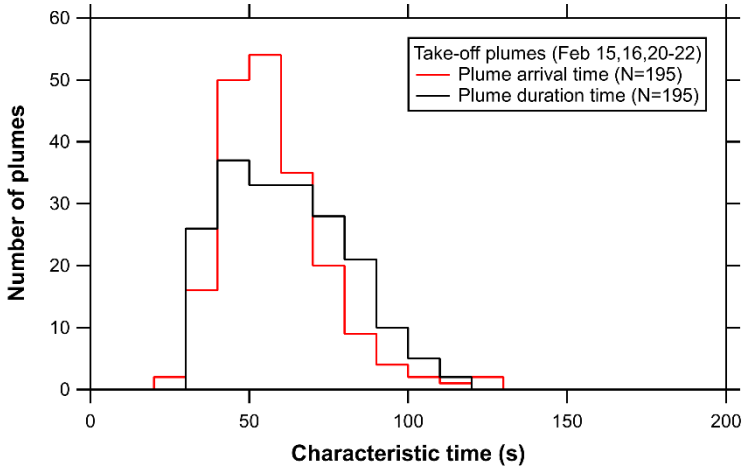


**Figure S~~24~~:** Histograms of the estimated arrival time and duration of plumes. The lower and upper limits of the duration time (30 s and 120 s, respectively) were determined by the definition of plumes.

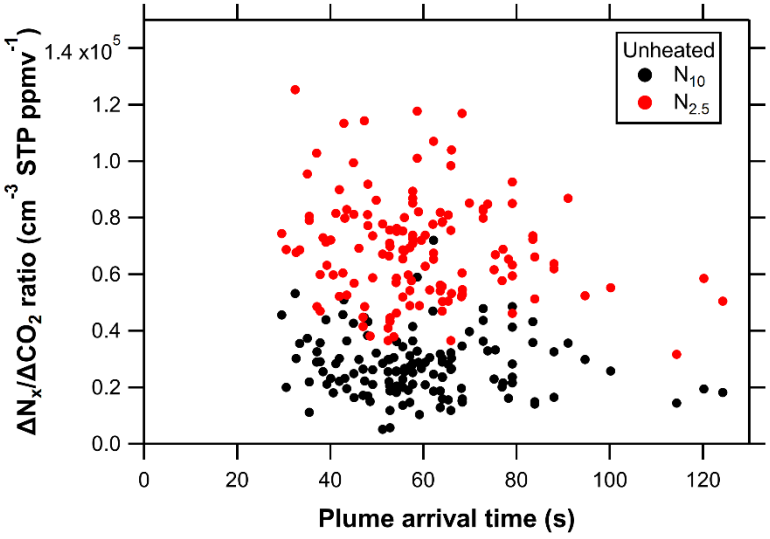


**Figure S~~35~~:** Dependence of $\Delta N_{2.5}/\Delta CO_2$ and $\Delta N_{10}/\Delta CO_2$ ratios on the arrival time of plumes.

**Table S~~1~~2:** Medians of particle number EIs for take-off plumes classified by major aircraft models identified in this study (~~the~~ number of samples ≥ 5). The unit of particle number EIs is $10^{15}$ kg-fuel$^{-1}$.

| Aircraft model | Total | | | | Non-volatile | | | |
|---|---|---|---|---|---|---|---|---|
| | Number of samples | EI($N_{2.5}$) | EI($N_{10}$) | Sub-10 nm fraction | Number of samples | EI($N_{2.5}$) | EI($N_{10}$) | Sub-10 nm fraction |
| A320 | 12 | 80 | 44 | 0.44 | N/A | N/A | N/A | N/A |
| A321 | N/A | N/A | N/A | N/A | 6 | 3.6 | 2.3 | 0.44 |
| A333 | 21 | 94 | 35 | 0.65 | 9 | 2.4 | 1.2 | 0.49 |
| B738 | 9 | 117 | 45 | 0.56 | N/A | N/A | N/A | N/A |
| B748 | 5 | 114 | 41 | 0.66 | N/A | N/A | N/A | N/A |
| B763 | 14 | 129 | 50 | 0.64 | 11 | 9.4 | 1.8 | 0.66 |
| B772 | 7 | 91 | 26 | 0.71 | N/A | N/A | N/A | N/A |
| B77W | 15 | 96 | 34 | 0.65 | 9 | 2.7 | 1.3 | 0.49 |
| B788 | 10 | 139 | 71 | 0.54 | N/A | N/A | N/A | N/A |
| B789 | 12 | 125 | 64 | 0.54 | N/A | N/A | N/A | N/A |

N/A: Not available.